SSRG International Journal of Civil Engineering
ISSN: 2348-8352/ https://doi.org/10.14445/23488352/IJCE-V13I10P114

Volume 13 Issue 10, 211-240, October 2026
© 2026 Seventh Sense Research Group®

*Original Article*

# Evaluation and Analysis of a Novel Fugitive Road Dust Collector and Its Prediction Using Machine Learning Models

Dipak G. Mangrulkar[1*], Prashant Y. Pawade[1], Mangesh P. Bhorkar[1]

[1]*Civil Engineering Department, G. H. Raisoni College of Engineering, Nagpur, Maharashtra, India.*

[*]*Corresponding Author: mangrulkardipak@gmail.com*

Received: 09 July 2026 Revised: 12 October 2026 Accepted: 20 October 2026 Published: 28 October 2026

***Abstract*** *- This research paper presents the conceptual design, development and performance evaluation of a compact fugitive vehicular dust collector to control and mitigate air pollution resulting from increased particulate matter on roadways. The developed dust collector is designed to work with two-wheeler automobiles, having a length 0.3 m, 0.15 m in diameter, and weight 2Kg, was experimentally tested on the gravel, asphalt, and concrete road at different speed of the vehicle. Results show distinguished dust collection efficiencies of 67.29% for gravel road, 65.65% for asphalt road, and 33.26% for concrete road, with dust collection increasing proportionally with speed of vehicle and maximum dust collection of 480 g at 80 km/h. The aerodynamic study verifies that dust jet length and mudguard dust area circumference expand as speed increases. The dust angle of attack increases from 220 at 20 km/h to 300 at 80 km/h, representing the direct relationship between speed of vehicle and dust dispersion pattern. The mathematical models were developed for gravel, asphalt and concrete road, reaching high correlations ($R^2$ > 98%), and machine learning approaches (Random Forest and XGBoost) further validated the accuracy of dust collection predictions. Relative assessment shows that gravel roads produce the more capturable dust, nearly 3% more than asphalt road and 35% more than concrete road. The dust collector is user-friendly, cost-effective (Rs. 7500 per unit, 83.94USD), and required very less maintenances with easy dust disposal. the mobile dust collector reduces fugitative particulate matter and minimises dust air pollution and provides a practical and scalable way to improve air quality, environmental sustainability and community health.*

***Keywords*** *- Fugitive Dust, Design of Dust Collector, Environmental Air Pollution, Two Wheeler, Random Forest and XGBoost.*

## 1. Introduction

Fugitive road dust is a major source of particulate pollution, especially in urban areas where resuspension of loose material is settled on road surface is continuously induced by moving traffic. The quantity of resuspended dust depends on several interacting factors, including traffic volume, vehicle speed, road-surface condition, silt loading, moisture content, meteorological conditions, and surrounding activities. Conventional road-dust measurement techniques generally involve manual or stationary sampling, while mobile systems such as the Colorado State University dustometer have demonstrated the potential for collecting road-dust samples over larger road sections with improved sampling efficiency [1]. Similarly, the Wet Dust Sampler developed by Lundberg et al. provided a repeatable approach for quantifying road-surface dust under different surface and climatic conditions [2]. The need for improved road-dust measurement is particularly important in India because extensive field investigations have reported substantial spatial variation in road-surface silt loading across Indian cities [3]. In parallel, Machine Learning (ML) techniques provide an opportunity to establish nonlinear relationships between experimentally measured dust characteristics and influencing parameters, thereby enabling rapid prediction at locations where direct measurement is not available. Recent developments in data-driven environmental modelling further demonstrate the potential of ML for particulate-matter prediction and road-dust characterization. Therefore, the present study focuses on the evaluation and analysis of a novel fugitive road-dust collector and the development of machine-learning models for predicting road-dust characteristics, with the aim of developing a practical, efficient, and data-driven methodology for road-dust assessment.

Road dust is commonly found on road surfaces and their surrounding areas. It consists of organic and inorganic materials such as soil, stones, metals, and other debris generated by vehicle movement and human activities such as

This is an open access article under the CC BY-NC-ND license (http://creativecommons.org/licenses/by-nc-nd/4.0/)

construction [4]. Road dust may also contain particles from road-marking paints, plastics used in road construction, and tyre and brake wear [5, 6]. Vehicle movement can resuspend these particles into the atmosphere, while rainfall and surface runoff can transport them into nearby water bodies [7]. Figure. 1 shows vehicles travelling on a rough, unpaved road, producing dust clouds that can deteriorate air quality. Wind can further transport fine road-dust particles over considerable distances [8].

Road dust affects human health for inhalation, ingestion, and also effect the skin when in contact, and it is much vulnerable for children who have frequent hand-to-mouth contact [9]. The Particulate Matter (PM), which has solid and liquid droplets present in the atmosphere [10]. The $PM_{10}$ indicate that the particulate matter consist of 10 µm in diameter or less than that. Whereas $PM_{2.5}$ indicates the matter less than or equal to 2.5 µm [11, 12]. SEM is commonly used to examine particles that cannot be observed with the naked eye.

Tyres contain polymers, carbon black, fibres, steel wires, fillers, and other organic and inorganic materials [13]. Continuous tyre–road contact produces wear particles that can contribute significantly to road dust and $PM_{10}$ emissions [14]. Higher temperatures at the tyre surface may promote the formation of finer $PM_{2.5}$ particles, whereas mechanical abrasion and shear mainly generate larger $PM_{10}$ particles [15]. Figure 2 illustrates a cross-section of a Water Bound Macadam (WBM) road and the movement of dust particles caused by vehicle activity and environmental processes.



**Fig. 1 Real-time view of road dust**

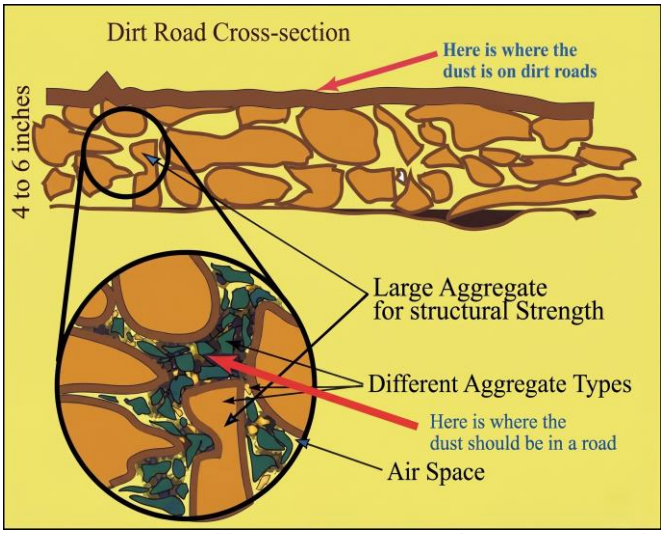



**Fig. 2 Mechanism of formation and presence of dust on x-section of WBM road surface [15]**

The main layer, approximately 4 to 6 inches thick, consists of both large and small aggregates. To keep the road stable, fine dust particles should fill the cracks between aggregates. But the picture suggests that the dust is left loose on the surface, which causes pollution and erosion. To understand how dust collection is accomplished, an initial literature review was conducted. A literature review provides an overview of the existing research on road dust collectors. It demonstrates the existing designs, their limitations. The following section illustrates the key findings of the literature review.

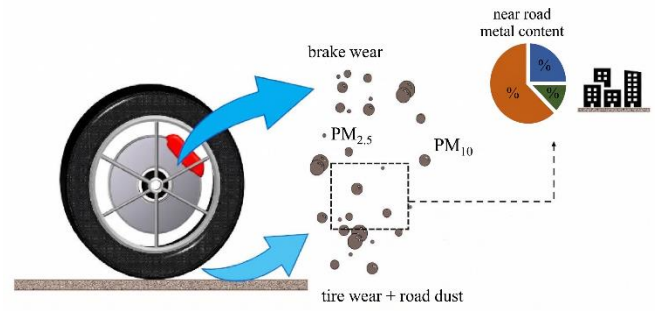



**Fig. 3 Generation of road dust by vehicle tyre [17]**

## 2. Literature Review

From the literature, it has been observed that several investigators have employed innovative methods to collect dust and studied the ill effects of inhaling it. According to [16], the chemical composition of tyre tread and tyre dust has been compared in several studies. The results showed that tyre dust contains higher concentrations of heavy metals such as Fe, Ti, Zn, and Cu, which may originate from brake wear and asphalt pavement materials. Researchers have also investigated the size, shape, and chemical composition of particles generated under laboratory conditions and collected from actual roads during simulated driving tests [13–17]. It is observed from

Figure 3 that the formation of $PM_{2.5}$ and $PM_{10}$ are formed through moving vehicle tyres and also from brake wear, along with road dust. This is the main effect of air pollution, which contains metals in the particles of the surrounding roadways.

In the construction of the road, both asphalt and concrete are most widely used materials. Asphalt mixture consist of 5% of bitumen and 95% of mineral aggregates. The bitumen is derived from crude oil, which consists of hydrocarbons and their derivatives, which is black in color, and it is a highly viscoelastic material [18]. The concrete pavement is a mixture of cement, Fine Aggregate (FA) and Coarse Aggregate (CA). Figure 4 illustrates the internal structure of asphalt concrete, comprising rock particles, a bituminous binder, and air spaces. A good balance of these parts makes the road last longer, able to hold more weight, and less dust comes from wear on the surface.

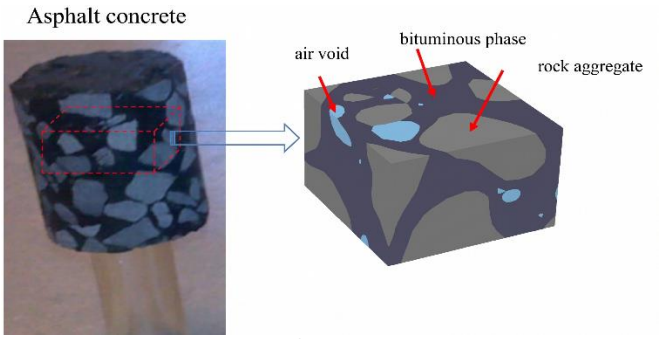



**Fig. 4 Material composition of a common asphalt concrete mixture**

Road wear can release organic compounds from asphalt into the atmosphere, contributing to the formation of secondary aerosol particles [19]. The different stone fractions present in pavement materials can also generate mineral particles containing elements such as Ca, Si, Fe, K, and Al [20]. Several studies have used different analytical methods to distinguish particles produced by road surface erosion from those generated through the resuspension of previously deposited road dust. Figure 5 illustrates how wind moves soil particles of different sizes: large ones crawl, medium ones bounce (saltation), and small particles remain suspended in the air for short or long distances, which contributes to dust pollution and erosion.

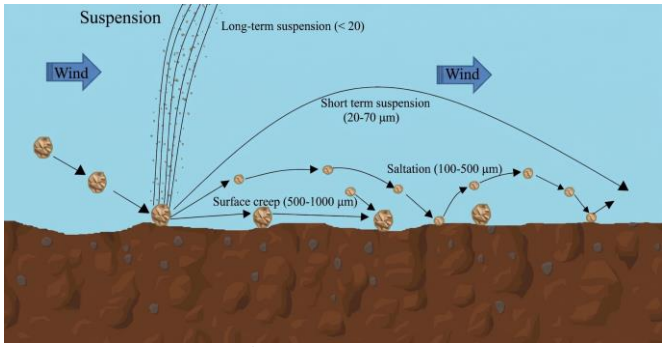



**Fig. 5 Dust formation and suspension [20]**

Various researchers have discovered bitumen as a possible tracer for particles brought forth through road wear [21–23]. The road particles are mainly because of airflow, turbulence and tyre movement, which is produced from the vehicles, which is the main source of non-exhaust particulate emission [24]. The composition of road dust can vary considerably with climatic conditions, soil disturbance, terrain characteristics, and human activities. The particles may originate from either natural or anthropogenic sources [25]. X-ray diffraction (XRD) has been widely used to examine the mineralogical characteristics of road dust. Studies reported in [26–28] identified significant amounts of inorganic elements, including Pb, Fe, Zn, Sn, Cu, and Sb, in road-dust samples. A spinning side brush (Figure 6) on the road dust collector sweeps dirt into the centre, where a vacuum system collects it. It cleans city streets effectively when mounted near the back tyre, but it's less effective at capturing dust in real-time when in motion.



**Fig. 6 Spinning brush–type road dust collector [28]**

Road dust can pose health risks because it may contain toxic elements such as lead and chromium, which can enter the human body through inhalation [29]. Lead exposure has been associated with impaired cognitive and neurobehavioral development, particularly in children [30]. It has also been linked to reproductive problems [31], chronic kidney disease, hypertension, and microcytic anaemia. Franklin et al. [32] reported an association between exposure to $PM_{2.5}$ and cardiovascular mortality. Road-dust exposure may also aggravate respiratory symptoms in people with asthma [33]. In addition, soluble platinum present in road dust may enter the body through contaminated food or water and has been associated with potential carcinogenic effects [34]. Studies have further reported relatively high concentrations of arsenic in road dust collected from industrial and commercial areas [35].

The point close to the vehicle's bottom, beyond the front wheels, was where the most resettled road dust was collected in both the computational and experimental studies. In contrast, additional dust was sampled at greater vehicle speeds [36]. The designed and constructed cyclone separator has been operating as intended. With the necessary pressure generated

by the vacuum pump, it can efficiently separate particles up to 1.5 x 10-6 m in diameter. It has been demonstrated that utilising a cyclonic separator to mitigate diesel engine particle emissions without compromising fuel efficiency is a cost-effective and practical solution [37].

From Figure 7, it is observed that the cyclone generated a vortex to allow the dusty air from the side, which causes a centrifugal force on the particles against the walls, and it falls into the hopper where the purified air leaves through the top.

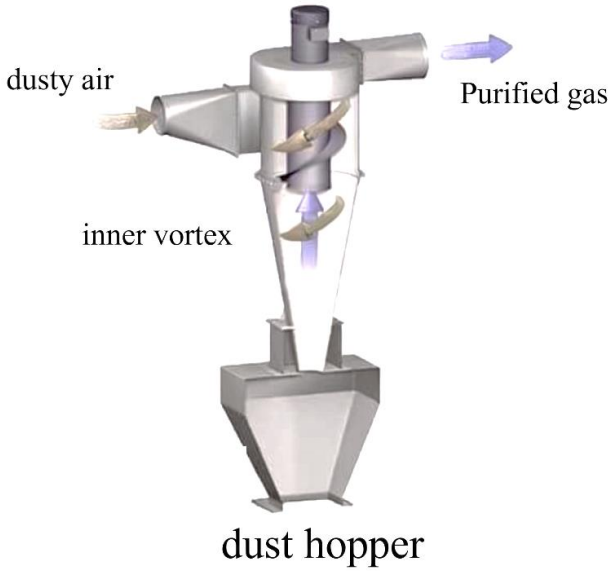



**Fig. 7 Cyclone-type road dust collector [37]**

The usage of air purifiers is merely a minor step in the long-term process of improving the air quality [38]. To reconcile both the upward and downward air pressures within the pickup head and capture entirely the dust particles, the air exiting the centrifugal fan is directed back toward the pickup head using a regeneration air sweeper airflow controller. A demonstration rig system was used to model and analyse the dust control system [39].

The increased wind velocity at the entry point is the cause of the dust collector's unequal flow rate dispersion. To standardise the internal flow field, a baffle plate was installed at the inlet. In this manner, the primary technical parameters, such as the maximum flow rate, unequal amplitude, and irregular amplitude, are reduced [40-46]. Figure 8 shows how dust from the road and particles from worn-out tyres harm the environment. It depicts how things like traffic, rain, and sun radiation may pollute the air and water by releasing things like PM, $NO_x$, $CO_2$, and black carbon, which can harm health and ecosystems.

From the literature review, the guidelines for dust collection air quality assessment and study related to real-time dust particle fluctuation and its effect on vehicle traffic volume are well presented in the literature [47]. It is observed that there is a lack of established protocols, techniques, and application standards for road dust collection, which limits the use of several existing pieces of equipment for quantifying particle concentrations and dispersion. Table 1 compares the existing methods for collecting road dust. Figure 9 illustrates various techniques for controlling dust, including sweeping, spraying, chemical suppressants, vegetation management, traffic management, paving, and the use of mobile samplers. Each approach is presented clearly and straightforwardly, illustrating how to reduce road dust and pollution effectively.

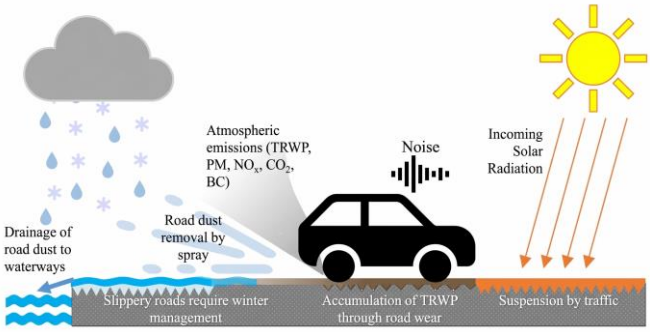



**Fig. 8 Dust from the road and particles from worn-out tyres harm the environment [46]**

Recent research has increasingly incorporated artificial intelligence and machine learning into dust monitoring and prediction. De Silva et al. demonstrated a deep-learning semantic-segmentation approach for identifying and quantifying traffic-induced dust from images, with the predicted dust characteristics being related to measurements from a research-grade monitoring instrument [48]. Ivanova et al. subsequently applied neural networks to predict toxic metals and metalloids associated with road-dust silt loading and reported high prediction accuracy for several elements, demonstrating the potential of ML to reduce dependence on repeated laboratory analysis [49]. More recently, machine-learning approaches have been extended to fugitive-dust emission estimation, with Song et al. using interpretable ML to identify important factors and nonlinear interactions affecting soil fugitive-dust emissions and subsequently improve localized emission calculations [50]. Particularly relevant to the present research, Chu and Shen reported in 2026 an explainable ML framework for predicting road silt loading using data from more than 300 roads across 28 Chinese cities; XGBoost, support-vector regression, and ensemble models were evaluated, while SHAP analysis was used to identify the influence of road class, precipitation, traffic characteristics, and other variables [51]. In another recent 2026 study, Bayesian-optimized CNN–LSTM networks were used to predict road-construction dust concentrations by integrating sensor, meteorological, and construction information, achieving an R2 of 0.884 [52]. These developments demonstrate the growing potential of data-driven methods for road and fugitive-dust prediction;

however, comparatively limited research has integrated a new physical road-dust collection device, systematic field validation, and machine-learning prediction using the collector-generated dataset. Therefore, the proposed study can address this gap by experimentally evaluating a novel collector and subsequently developing and validating ML models for predicting dust loading or collection efficiency from road, traffic, and environmental parameters.

Empirical models, such as the US EPA-42 guidelines (chapter 13.2.1 for paved roads and chapter 13.2.2 for unpaved roads), have been the standard for estimating the particulate emissions from roadways based on vehicle weight, speed and surface silt loading to estimate factors [53, 54]. However, this macro-scale empirical equation predicts the cumulative dispersion of fugitive dust into the atmosphere, not the localized capture dynamics at the wheel -road interface. Recent aerosol resuspension literature suggests that vehicle-induced particulate emissions are governed by two distinct aerodynamic mechanisms, namely mechanical tire shear and tire-wake turbulence [55, 56]. Rotating tires produced high-velocity shear stress and turbulent wake structures that resuspend settled particles into the undercarriage region [57]. While existing studies (e.g., mobile testing systems like TRAIN and SNIFFER) focus primarily on measuring this tire-wake emission flux, there remains a critical gap in developing active, vehicle-mounted mitigation systems designed to intercept and collect this resuspended dust directly at the source before ambient dispersion occurs.




**Fig. 9 Dust control methodologies**

### *2.1. Motivation behind the Present Research Work*

According to the previous study, numerous researchers have investigated the relationship between heavy metal accumulation and road dust density in the road surface. Some of them have also worked on a sampler for the collection and retrieval of dry dust deposition; however, very little work has been done on a dust emission controller for mobile equipment. Hence, the present work has been undertaken. In the present work, a cost-effective and portable device is designed to collect dust from the rear wheel of any two-wheeler, enabling the determination of PM2.5 and PM10 concentration on any road.

### *2.2. Specific Objectives of the Present Research Work*

The specific objectives of the present research are as follows:

a) To determine the quantity of dust emission.
b) To evaluate the parameters related to dust emission.
c) To prepare the equipment to collect and control the dust emission.
d) To assess and predict the dust collector's performance at different speeds using machine learning models.

### *2.3. Novelty of Present Research Work*

The proposed mobile dust-collecting sampler offers a novel, two-wheeler-mounted solution for controlling fugitive vehicle dust on roads. This mobile device is portable, unlike the large and non-portable fuel-powered vacuum trucks, and can filter particles in real-time. It offers a pragmatic and sustainable solution for dust control on roads in different conditions. The materials and methods employed in the present study are described in detail in the following section. It tells the exact components used to build the dust collection system. The type of filter used, the arrangement of the fan, the size of the ducts and the location of the fans motor.

## 3. Materials and Methodology

Materials and methods are very essential because they clarify how the research was conducted, confirming that the findings are precise and can be simulated. This section shows the detailed outline of the materials and methods which are used to carry the present research work.

### *3.1. Materials*

The mobile vehicular dust collector is fabricated with PVC material, which is light in weight, cost-effective and easy to install for any two-wheeler dust collection. The detailed fabrication model is given in Figure 10 and 15. To restrict the larger particles, a fine mesh is attached at the inlet, also HEPA is installed for finer PM particles. The air velocity in the duct (V = 15 m/s) was measured by means of a hot-wire anemometer, the rotational speed of the fan was measured by a digital laser tachometer, and the pressure drop across the HEPA filter was measured by a digital differential pressure manometer (differential pressure gauge). An RS-775 DC motor is powered by a 12-volt battery.

It powers a fan with plastic blades, as shown in Figure 10, generating the necessary suction to draw in dusty air and release clean air. PVC end caps are used to enclose the setup, ensuring the correct direction of airflow. While nuts, bolts, and screws hold all the parts firmly in place, clips and fasteners—made of metal are used to attach the system to the vehicle securely. The equipment is practical, portable, and suitable for reducing vehicle dust emissions.

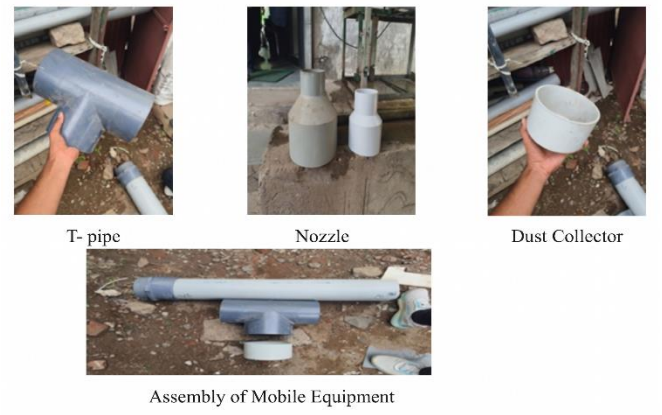



**Fig. 10 Material and part of the mobile dust sampler**




**Fig. 11 Components and Assembly of the Two-Wheeler-Mounted Dust Collection Sampler**

### *3.2. Attachment method on the Vehicle*

Figure 11 displays metal clamps, brackets, and cable ties used to firmly fasten the mobile dust collection sampler to the two-wheeler, adjacent to the rear tyre. The steel structure is fixed on the footrest on the rear side leg guard. It supports the dust collector device steady, even while the vehicle is in motion. This arrangement enables the dust collector to be positioned close to the road surface, effectively gathering the dust particles generated.

The air first passes through a fine mesh screen (primary filter), which removes larger dust particles and coarse particles. A secondary HEPA filter, which filters out smaller particles like $PM_{10}$ and PM2.5, thus the air is cleaned and exits from the outlet into the atmosphere. The collected dust stays held inside the dust collector. This process is continued till the vehicle is in motion. The expenditure associated with the production of the dust collector is presented in Table 2.



**Fig. 12 Installation of a mobile dust collection sampler on two two-wheeler vehicles**

### *3.3. Methodology*

#### *3.3.1. Design Parameters*

During the development of a dust filter, airflow is taken into account because it helps determine the necessary air volume, air velocity, and pressure drop through the filter. The following procedures outline the steps to calculate dimensions with airflow.

a) Establish the necessary airflow to fix the size of suction fan
b) To determine the velocity of air passing across the filter from the tyre.
c) To estimate the effectiveness of the Filter.
d) To calculate the area of the filter.
e) Identify the suitable filter material.
f) To finalize the dimensions of the filter.
g) Developed model was tested for the dust collection at various speeds of the vehicle.

#### *3.3.2. Design of Dust Collector*

The dust-collecting system on a moving vehicle utilises a suction intake to capture dust particles from the air. The drag force, aerodynamic lift and gravitational weight are the three basic factors that affect the velocity of each dust particle.

Figure 12 shows that the drag force acting on the particle is approximately ($9.824 \times 10^{-9}$) N, opposing its relative motion with respect to the surrounding airflow. The aerodynamic lift force is approximately ($6.3 \times 10^{-15}$) N, acting perpendicular to the airflow and potentially influencing the particle's vertical trajectory. Meanwhile, the gravitational force (weight), calculated as (W=mg), acts vertically downward. The combined effects of drag, lift, and gravity govern the particle's trajectory and its potential entry into the dust collector.

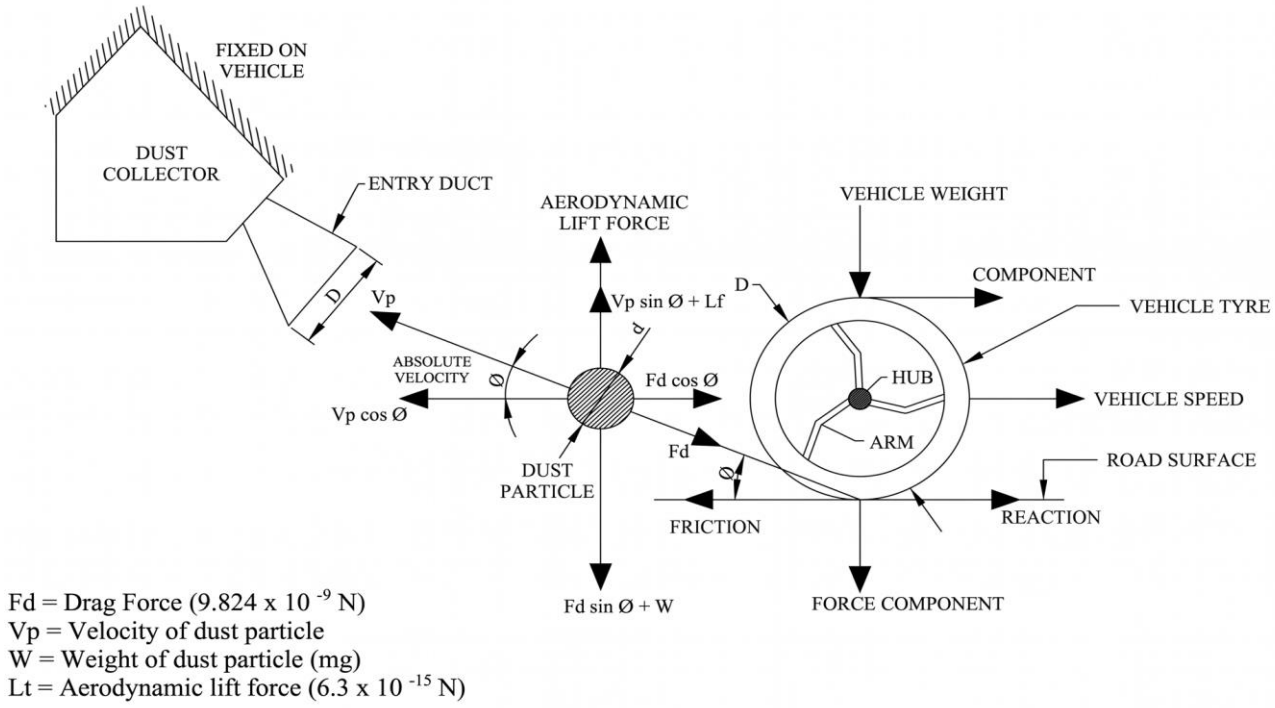
Figure 13 illustrates how these forces are composed of vectors. The particle's speed, $Vp$, is at an angle of Φ and its horizontal and vertical parts are $Vp\cos\Phi$ and $Vp\sin\Phi$. The drag force breaks down into $Fd\cos\Phi$ and $Fd\sin\Phi$, and the vertical balance has both lift and weight: $Vp\sin\Phi + Lf$ upward and $Fd\sin\Phi + W$ downward.

These forces work together to decide whether the dust particle will follow the airflow to the inlet of the dust collector.

Tables 3 and 4 illustrate the estimated dimensions of various parts of the road dust collector

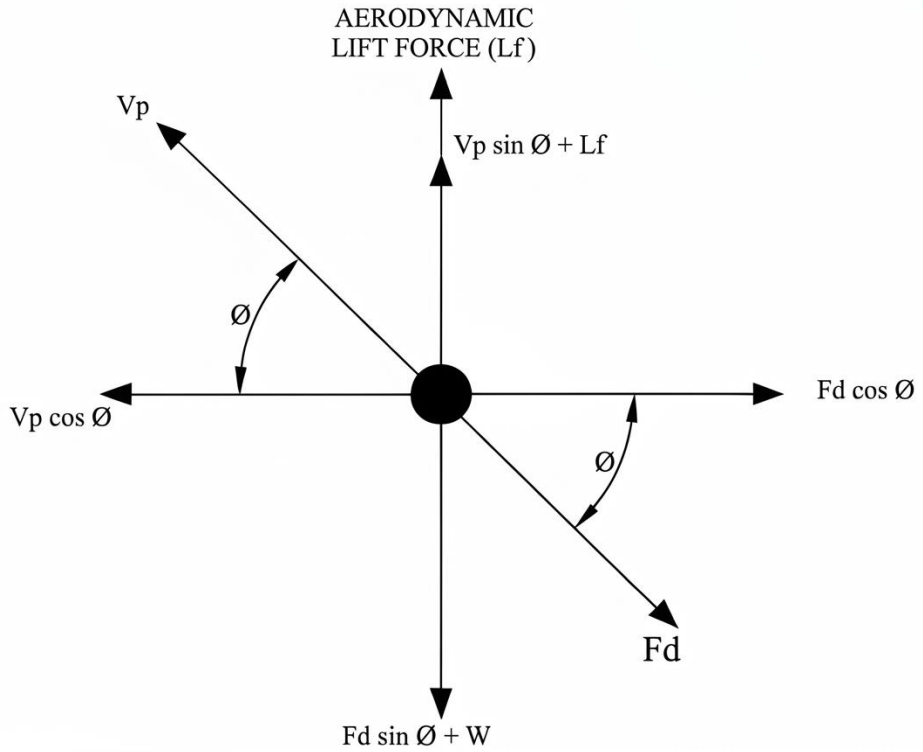
**Table 2. Cost Analysis**

| Sr. No. | Component / Description | Specification / Technical Details | Quantity | Unit Cost (₹) | Total cost (₹) |
|---|---|---|---|---|---|
| 1 | PVC Pipe (110 mm, 3 ft) | Central duct for dust suction; rigid PVC, 110 mm diameter, 0.9 m length | 1 | 218 | 218 |
| 2 | PVC Tee (110 mm) | T-joint for connecting suction duct to main chamber; heavy-duty PVC | 1 | 218 | 218 |
| 3 | PVC End Cap (110 mm) | Used for sealing duct ends and filter housing | 2 | 95.5 | 191 |
| 4 | PVC Reducer (110 mm to 50 mm) | Reduces section for fan outlet; improves air velocity | 1 | 75 | 75 |
| 5 | 775 DC Motor | 12–24 V, 7000–9000 rpm brushed motor, Ø5 mm shaft | 1 | 300 | 300 |
| 6 | Wire and Clips | 1.5 mm² copper wire with insulated coating and mounting clips | 1 | 60 | 60 |
| 7 | Air Filter | Circular filter, 100 mm Ø, 90 µm particle filtration | 1 | 250 | 250 |
| 8 | Fan Assembly (with glue) | 6-blade plastic impeller, 80 mm diameter, bonded with epoxy | 1 | 250 | 250 |
| 9 | PVC Pipe (1.5 inch) | Flexible suction hose connecting the funnel to the main chamber | 1 | 150 | 150 |
| 10 | PVC Elbow (1.5 inch) | Smooth-radius elbow for airflow direction | 1 | 30 | 30 |
| 11 | Funnel | Polypropylene funnel, inlet Ø150 mm, collects road dust jet | 1 | 60 | 60 |
| 12 | Vehicle Attachment Clips | Metal brackets to mount the sampler on a two-wheeler frame | 2 | 15 | 30 |
| 13 | Nuts and Bolts | M6×25 mm stainless steel fasteners | 1 | 50 | 50 |
| 14 | Screws | Self-tapping screws for securing the motor and fittings | 1 | 50 | 50 |
| 15 | Fabrication / Assembly | Cutting, drilling, sealing and assembly work | 1 | 500 | 500 |
| 16 | Battery (12V DC, 7Ah) | Lead-acid rechargeable battery for DC motor | 1 | 1250 | 1250 |
| 17 | Subtotal (A) | | | | 3682 |
| 18 | Manufacturing Cost (20%) | Labour and process cost | | | 736.4 |
| 19 | Overhead Cost (10%) | Workshop electricity, consumables | | | 368.2 |
| 20 | Research and Development Cost (10%) | Design and testing cost | | | 368.2 |
| 21 | Sales and Admin (5%) | Documentation and administration | | | 184.1 |
| 22 | Subtotal (B = A + above costs) | | | | 5339 |
| 23 | Profit and Overhead (15%) | | | | 800.85 |
| 24 | Subtotal (C = B + Profit) | | | | 6139.85 |
| 25 | Goods and services tax (GST) @18% | Applicable tax | | | 1105.2 |
| 26 | Final Selling Price (D = C + GST) | Total selling price of the equipment (round off) | | | 7500 |




Fd = Drag Force (9.824 x 10 $^{-9}$ N)
Vp = Velocity of dust particle
W = Weight of dust particle (mg)
Lt = Aerodynamic lift force (6.3 x 10 $^{-15}$ N)

**Fig. 13 Drag force on the dust particle**




Fd = Drag Force (9.824 x $10^{-9}$ N)
Vp = Velocity of dust particle
W = Weight of dust particle (mg)
Lt = Aerodynamic lift force (6.3 x $10^{-15}$ N)

**Fig. 14 Forces on a dust particle composed of vectors**

**Table 3. Dust Collector Design**

| Design Focus | Formula / Inputs | Final Outcome / Decision |
|---|---|---|
| Flow Conditions | Target: $PM_{2.5}$ and $PM_{10}$ capture at 20–80 KMPH. Assumed particle diameter of 2.5 µm, air density of 1.2 kg/m³, and dynamic viscosity of $1.8 \times 10^{-5}$ Pa·s. | Designed to capture fine dust particles effectively under real-world driving conditions. |
| Airflow Rate | Formula: $Q = A \times V$. Filter area $A = 0.002$ m², suction velocity $V = 15$ m/s. | $Q = 0.002 \times 15 = 0.03$ m³/s. The chosen dust inlet diameter is approximately 5.1 cm. |
| Stokes Number | Formula: $St = (\rho_p \times d_p^2 \times U) / (18 \times \mu \times D)$. Assumed particle density $\rho_p = 2{,}500$ kg/m³, particle diameter $d_p = 2.5 \times 10^{-6}$ m, flow velocity $U = 15$ m/s, duct diameter $D = 0.051$ m. | $St \approx 0.02$, indicating particles follow airflow well—ideal for fine filtration. |
| Filter Thickness | Evaluated HEPA filter options and pressure drop versus thickness trade-offs. | Selected filter thickness of 2 cm for optimal balance between suction power and filtration efficiency. |
| Settling Time | Formula: $t = H / V_t$. Collector height $H = 0.12$ m, terminal settling velocity $V_t \approx 0.15$ m/s. | $t = 0.12 / 0.15 = 0.8$ seconds. Sufficient settling time for dust particles. |
| Collector Volume | Formula: $V = m / \rho$. Assumed dust mass $m = 1.65$ g $= 0.00165$ kg, bulk density $\rho = 0.0015$ kg/cm³ $= 1.5$ kg/L. | $V = 0.00165 / 1.5 \approx 0.0011$ L $= 1.1$ cm³. Chosen dimensions: 11 cm diameter and 12 cm height. |
| Fan Selection | Swept area formula: $A = \pi \times (R^2 - r^2)$. Outer radius $R = 0.0475$ m, hub radius $r = 0.02$ m. | $A \approx 0.0071$ m². Selected 6-blade curved fan made of lightweight plastic, 9.5 cm diameter, operating at 1,000–5,000 rpm. |

Considering all aspects of design and environmental conditions, a portable, lightweight fugitive vehicular dust collector for two-wheelers has been fabricated. The dust collector line diagram is shown in Figure 15. A clear and detailed view of the dust collector, including labels, is presented in Figure 16 (disassembly). The workflow of this fugitive vehicular dust collector is shown in Figure 17 and Figure 18.

**Table 4. Summary of Optimised Dimensions**

| Component | Dimension / Value |
|---|---|
| Duct Diameter | 5 cm |
| Filter Area | 0.002 m² |
| Filter Thickness | 2 cm |
| Chamber Height | 12 cm |
| Chamber Volume | 1140.398 cm³ |

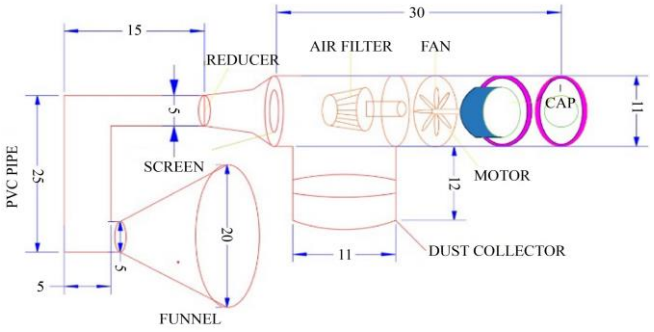



**Fig. 15 Fugitive vehicular dust collector**

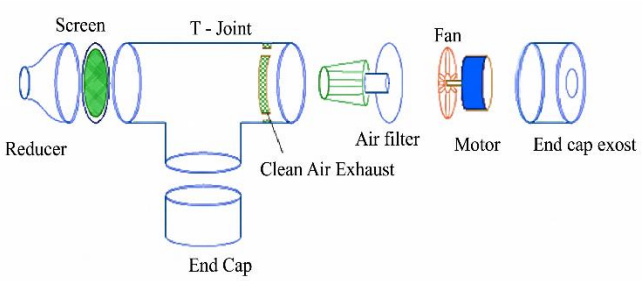



**Fig. 16 Exploded view of the fugitive vehicular dust collector.**

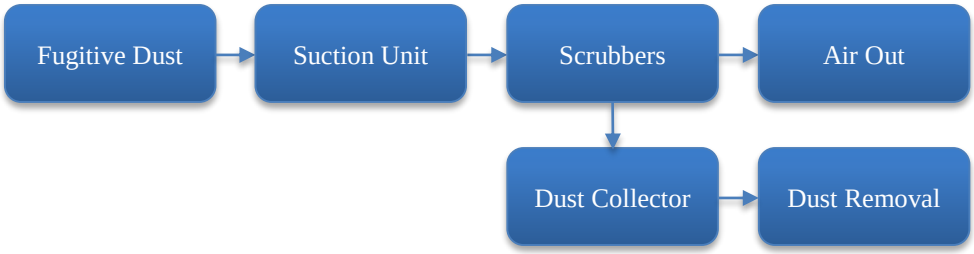



**Fig. 17 Working of a dust collector**



**Fig. 17 Fugitive vehicular mobile dust collector prototype (actual)**

To assess the feasibility of the designed air dust collector, it is essential to evaluate its performance in actual working conditions. So, the following points are considered depending on the literature reviewed and discussed in the earlier section of this manuscript for experimental/actual testing of this fugitive vehicular dust collector.

- Site Selection (Road)
- Vehicle Selection (Motorcycle/moped/scooter, etc., since tyre size will affect dust spreading)
- Attachment of the Speedo meter to the rear wheel for the calculation of speed
- Taking readings at constant velocity 20 KMPH, 30 KMPH, 40 KMPH, 50 KMPH, 60 KMPH, 70 KMPH and 80 KMPH.
- Collection of dust samples at various constant speeds of the vehicle
- Measurement of collected dust at various constant velocities.

#### *3.3.3. Aerodynamic Drag and Motor Power Consumption*

The aerodynamic effect of mounting the dust collector on the two-wheeler was considered to assess whether the additional equipment causes any significant resistance during vehicle operation. The dust collector was securely mounted near the rear wheel, and the vehicle was operated at the selected test speeds of 20, 30, 40, 50, 60, 70 and 80 km/h. The additional drag associated with the mounted equipment was assessed based on the operating condition of the vehicle with the dust collector attached.

The power consumption of the RS-775 DC motor was also considered during continuous operation of the dust collection system. The motor was powered using the 12 V battery provided in the prototype. During operation, the electrical current drawn by the motor was measured using an appropriate current-measuring instrument, and the electrical power consumption was determined from the measured voltage and current. The motor was run continuously during the test period to determine its power requirement under working conditions. These measurements were used for the estimation of the real energy demand of the mobile dust collection system during the operation of the vehicle.

#### *3.3.4. Machine Learning Approach*

Random Forest (RF) and Extreme Gradient Boosting. For this study, XGBoost, also known as XGB, was used because of its known performance in modeling. The RF is an ensemble learning technique that combines the predictions of multiple decision tree models to control variance and avoid overfitting, and is suitable for moderate sized datasets with mixed feature types. XGB is a newer gradient-boosting framework, which was selected because it can model subtle patterns by additive tree-based learning, and adds regularization to control the complexity of models.

The dataset comprised 210 samples experimentally obtained under moderate environmental and ambient moisture conditions. Preprocessing steps involved one-hot encoding of categorical variables, standardization of numerical features, and imputation of missing values with the median. Outliers were detected and removed using the Interquartile Range (IQR) method. The experimental data were randomly divided into (80%) and a testing (20%) subset. A 5-fold cross-validation scheme was applied during hyperparameter tuning to ensure robustness and avoid overfitting. The models were implemented using the scikit-learn library for RF and the XGBoost library for gradient boosting.

Hyperparameters were optimised using a grid search approach. The RF model used 100 decision trees (estimators), a maximum depth of 10, and a minimum sample split of 5. The XGB model performed the best with 200 estimators, a maximum depth of 8, a learning rate of 0.1, and subsample and colsample_bytree rates of 0.8. Using the test set that was not visible, performance metrics, including the coefficient of determination ($R^2$), Mean Absolute Error (MAE), and Root Mean Squared Error (RMSE), were evaluated.

## 4. Experimental Investigations, Results and Discussion

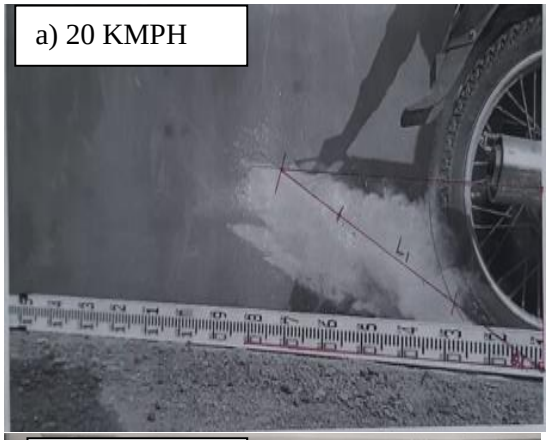
### *4.1. Collection of Dust at Different Speeds of a Two-Wheeler Vehicle*

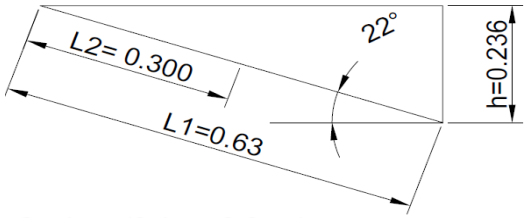
The prototype model (Figure 18) is attached to the Splender, a two-wheeler vehicle. The fugitive dust is collected from Water-Bound Macadam (WBM) road behind the Mechanical Workshop of Bajaj Institute of Technology, Wardha (20.7453° N, 78.6022° E), at various speeds, including 20 km/h, 30 km/h, 40 km/h, 50 km/h, 60 km/h, 70 km/h, and 80 km/h, for stagnation testing.

Various trials are conducted, as shown in Figure 19, to collect dust emitted from the back side of the vehicle at the idle position. The purpose is to calculate the length of the jet, angle of the jet, dust collection, and to assess the performance of the prototype.

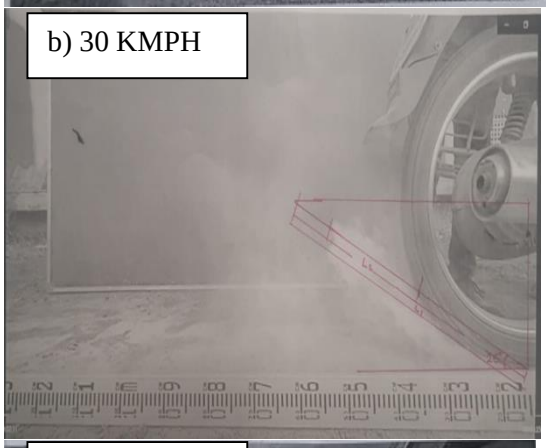


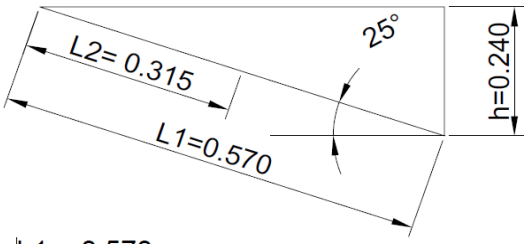

**Fig. 19 Investigation for location to mount the prototype on the vehicle (a) Behaviour of Jet (b) Dust collection**



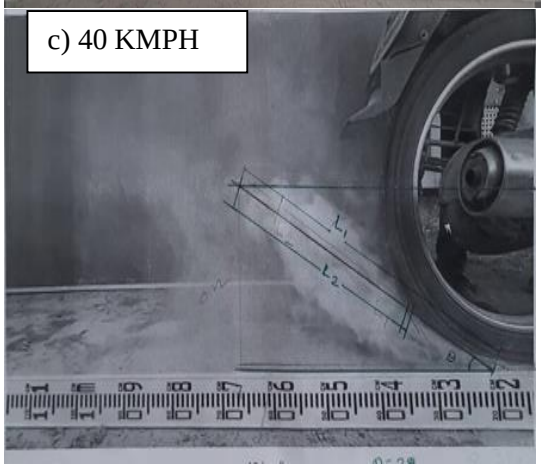



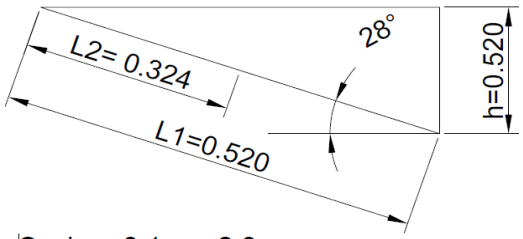

Scale :- (0.1m =2.2cm)
L1 = 14 cm = 0.63m
L2 = 06 cm = 0.3m
M = 60gm
V = 20Kmph
Θ = 22°
h = 5.2cm = 0.236m



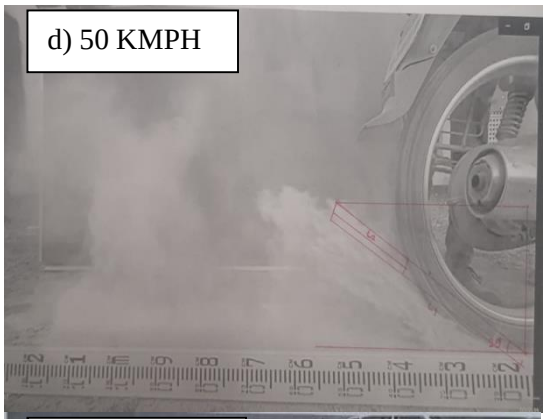



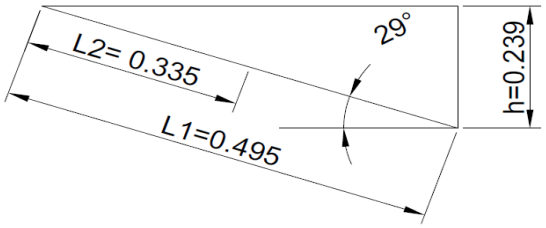

L1 = 0.570m
L2 = 0.315m
M = 105m
V = 30Kmph
Θ = 22°
h = 0.240m



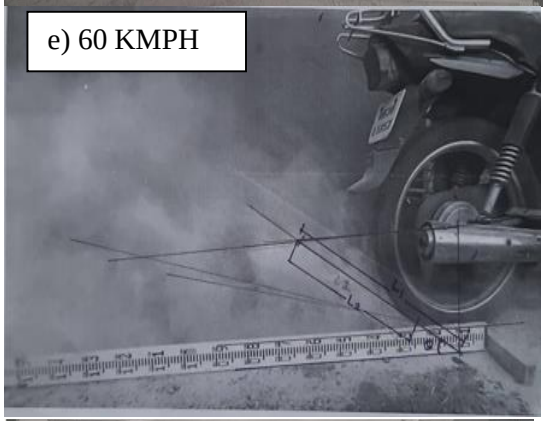



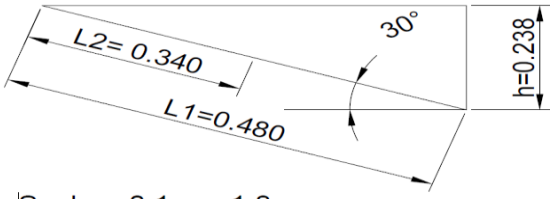

Scale :- 0.1m = 2.8cm
L1 = 0.520m
L2 = 0.333m
M = 15m
V = 40Kmph
Θ = 28°
h = 0.520m



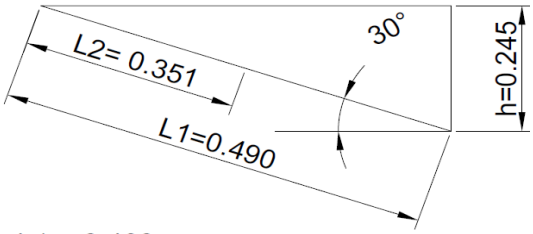

L1 = 0.335m
L2 = 0.495m
M = 220m
V = 50Kmph
Θ = 29°
h = 0.239m



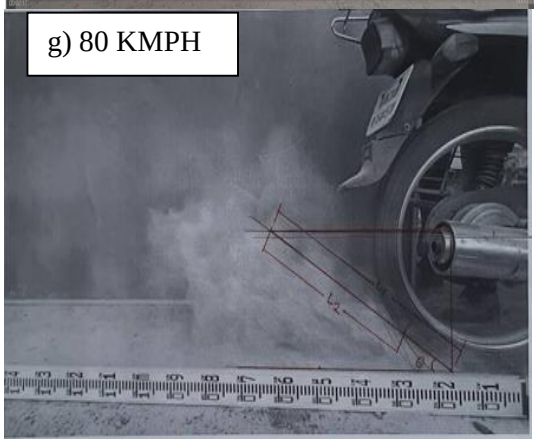



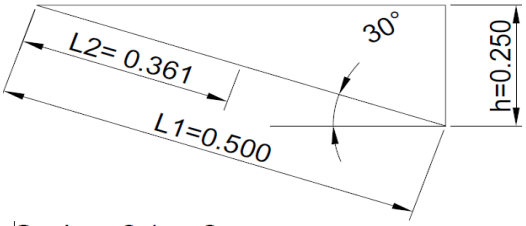

Scale :- 0.1m = 1.8cm
L1 = 0.480m
L2 = 0.34m
M = 290m
V = 60Kmph
Θ = 30°
h = 0.238m




L1 = 0.490m
L2 = 0.351m
M = 385m
V = 70Kmph
Θ = 30°
h = 0.245m




Scale :- 0.1m=2cm
L1 = 0.500m
L2 = 0.361m
M = 480gm
V = 80Kmph
Θ = 30°
h = 0.250m

**Fig. 20 Investigation for the actual angle of jet coming from the vehicle at different speeds**

Figure 20 illustrates the formation and behaviour of dust jets generated by a vehicle's tyre as it moves through a surface at different speeds, ranging from 20 KMPH to 80 KMPH. As the vehicle increases speed, the dust jet gets more scattered and projects farther from the tyre, exhibiting more force and turbulence. The careful observations in Figure 20 demonstrate how the spray outline changes at each speed tier, accompanied by calculated dimensions of spray height, length, and flight angle. Driving at lesser speeds of 20–40 km/h keeps the dust comparatively focused nearby the wheel area. Contrariwise, moving at a higher speed of 50–80 km/h blows out the particulate plume over a much larger area. The order in Figure 19(a–g) brings to light how increasing velocity upgrades the jet angle while lifting and propelling dust over greater horizontal and vertical distances. The quantity of dust collected over a set duration is detailed in Table 5 across different speeds. The table categorizes four main data points: speed (km/h), container mass before testing (g), container mass after testing (g), and the final net weight of the collected dust (g). Higher vehicle speeds result in a greater collection of airborne dust particles, which reveals a direct correlation between vehicle speed and dust accumulation.

**Table 5. Speed versus accumulated dust**

| Sr No | Speed of Vehicle (KMPH) | The dust's initial mass Container(g) | Final dust container mass containing the sample (g) | The sample's actual mass (Final - Initial) (g) |
|---|---|---|---|---|
| 1 | 20 | 400 | 460 | 60 |
| 2 | 30 | 400 | 510 | 110 |
| 3 | 40 | 400 | 550 | 150 |
| 4 | 50 | 405 | 615 | 210 |
| 5 | 60 | 410 | 700 | 290 |
| 6 | 70 | 410 | 805 | 395 |
| 7 | 80 | 410 | 890 | 480 |

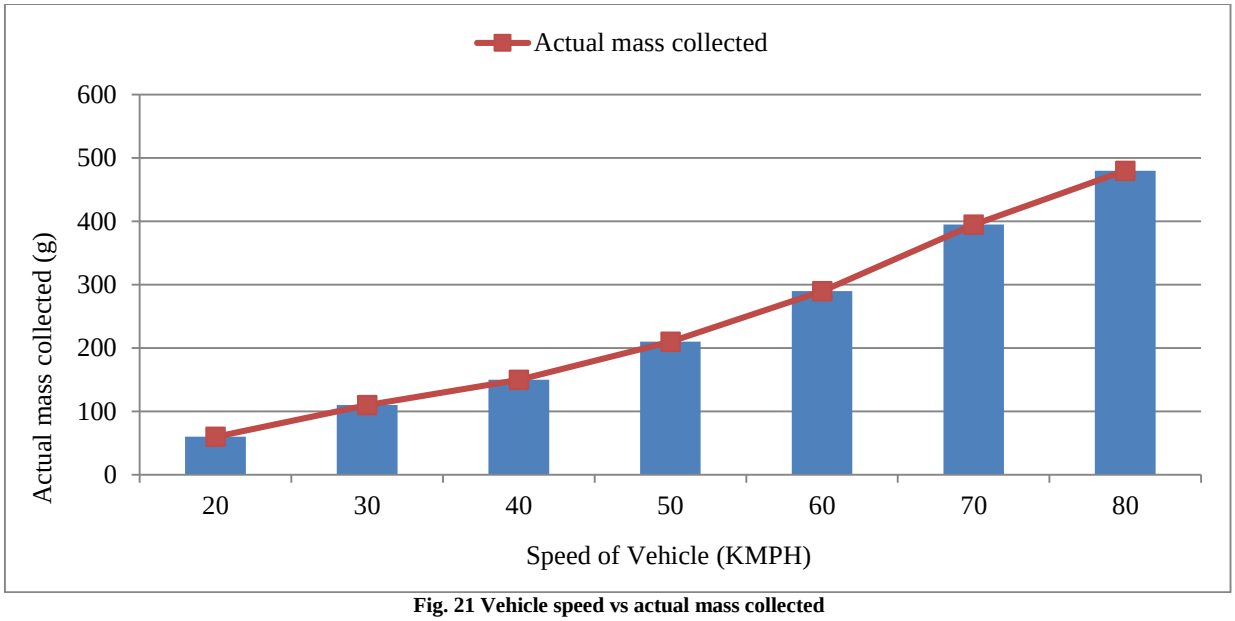



**Fig. 21 Vehicle speed vs actual mass collected**

As vehicle speed increases from 20 to 80 km/h (Figure. 21), the collected dust mass consistently increases from 60g to 480g. The rate of dust accumulation also increases progressively with an average increase from 45g, 70g, and 95g for 10KMPH over 20-40KMPH, 40-60KMPH, 60-80KMPH range, respectively.

This upward curving trend indicates progressively greater dust resuspension and collection at higher vehicle speeds, which may be attributed to enhanced tyre road interaction and aerodynamic turbulence.

At 20 KMPH, 60 g of dust are collected, and at 40 KMPH, 150 g. Following the pattern, the collected dust masses 290 g at 60 KMPH and 480 g at 80 KMPH. The pattern is that the higher the speed, the more turbulence is generated, and therefore the more dust is lifted and deposited in the container.

Similar trends are also reflected in the literature cited for the evaluation of the aerodynamic properties and airborne particulate matter of vehicular movement [36-43]. This finding is supported by recent studies on the effects of particulate matter emissions on air quality [42, 43].

Understanding the physics of dust distribution is crucial. With an R2 value of 0.9751, or 97% accuracy, Equation 1 shows a linear relationship between vehicle speed (x) and dust accumulation (Y).

$$Y = 7.00x - 105.00 \quad (1)$$

Table 6 considers the effects of speed by considering more aerodynamic parameters like angle of attack, maximum dust jet length, and dust particle diameter. As shown in Table 6, the vehicle velocity changes the dynamics of dust dispersion and collection. One of the parameters in Table 6 is the angle of attack (θ), which is the inclination of the dust particles relative to the air stream, as shown in Figure 22.

The angle of attack is 22 ° at 20 km/h. At 80 km/h, the angle of attack goes up to 30 °. This means that the faster the vehicle moves, the more dust particles change their direction. The dust particles also spread more and stay in the air longer.

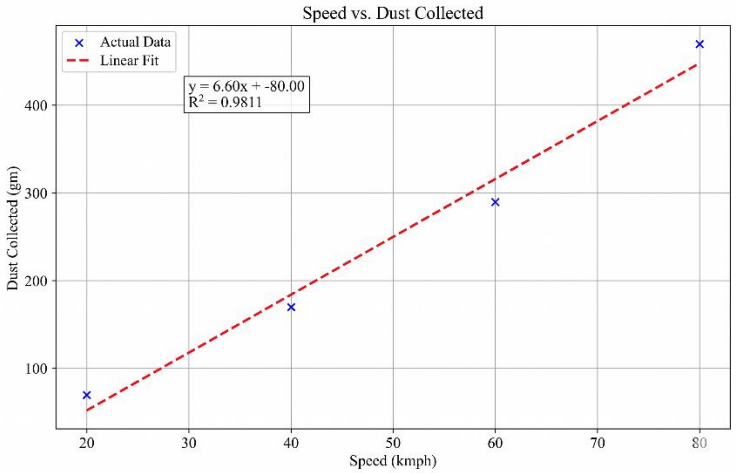



**Fig. 22 Speed vs dust collected**

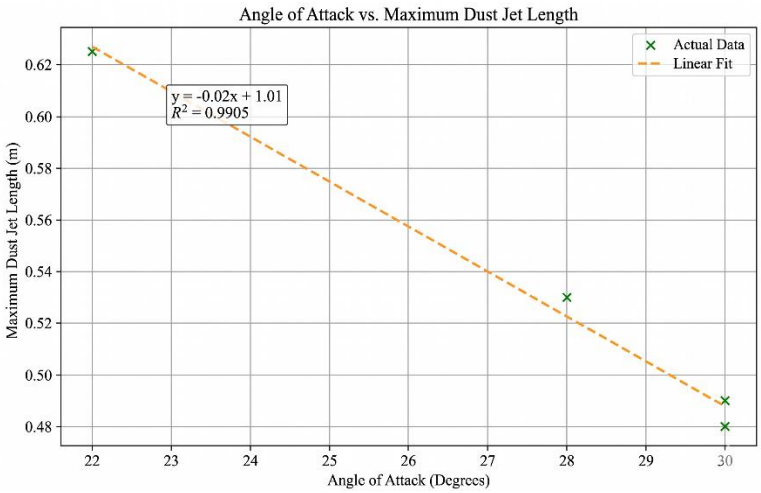



**Fig. 23 Angle of attack vs Maximum Dust of Jet Length**

The maximum dust jet length (L1) of the vehicle also follows the same trend as shown in Table 6, where it remains constant at 0.50 m at 80 KMPH after a slight fall at mid-range speeds. The jet mud guard circumference (L2) monotonically grows from 0.30 m at 20 km/h to 0.36 m at 80 km/h, showing the same positive correlation with speed. It implies that higher velocities lead to a greater extent of dust dispersion and implications for dust mitigation practices in off-road and construction environments. Moreover, the quantity of dust collected in 10 seconds increases significantly from 60 g at 20 KMPH to 480 g at 80 KMPH, following the same trend as shown in Table 6. Note that all the speed levels have the same dust diameter and dust collector length. It indicates that the size of individual dust particles does not change significantly, but speed influences the amount of dust collected and its distribution pattern, which confirms the results of the studies on environmental dust [41]. The linear regression of angle of attack (x) and maximum dust jet length (Y) is illustrated in Figure 22 and the corresponding Equation 2 with $R^2 = 0.9734$ (97% accuracy).

$$Y = -0.02x + 1.02 \quad (2)$$

From Table 6, it is clear that as the speed increases, the amount of dust collected also increases. The maximum dust collected is 480g at 80KMPH speed. The angle of attack for dust are also approximately of the exact nature for all the velocities and their jet lengths. From Table 6, it is clear that as the speed increases, the amount of dust also increases. The maximum dust collected is 480g at 80KMPH speed. The angle of attack for dust are also approximately of the exact nature of all the velocities and their jet length.

**Table 6. Different parameters at various velocities**

| Vehicle Velocity (V) KMPH | Diameter of filter D (m) | Dust Angle of attack θ (Degree) | Maximum length of dust jet, $L_1$ (m) | Length of jet mud guard circumference, $L_2$ (m) | Dust collected in 10 sec, (g) | Dust Plume diameter, Dd (m) | Mobile Equipment length (L/D=2), $L_f$ M |
|---|---|---|---|---|---|---|---|
| 20 | 0.43 | 22 | 0.63 | 0.30 | 60 | 0.15 | 0.30 |
| 30 | 0.43 | 25 | 0.57 | 0.31 | 110 | 0.15 | 0.30 |
| 40 | 0.43 | 28 | 0.51 | 0.33 | 150 | 0.15 | 0.30 |
| 50 | 0.43 | 29 | 0.495 | 0.33 | 210 | 0.15 | 0.30 |
| 60 | 0.43 | 30 | 0.48 | 0.34 | 290 | 0.15 | 0.30 |
| 70 | 0.43 | 30 | 0.49 | 0.35 | 395 | 0.15 | 0.30 |
| 80 | 0.43 | 30 | 0.50 | 0.36 | 480 | 0.15 | 0.30 |

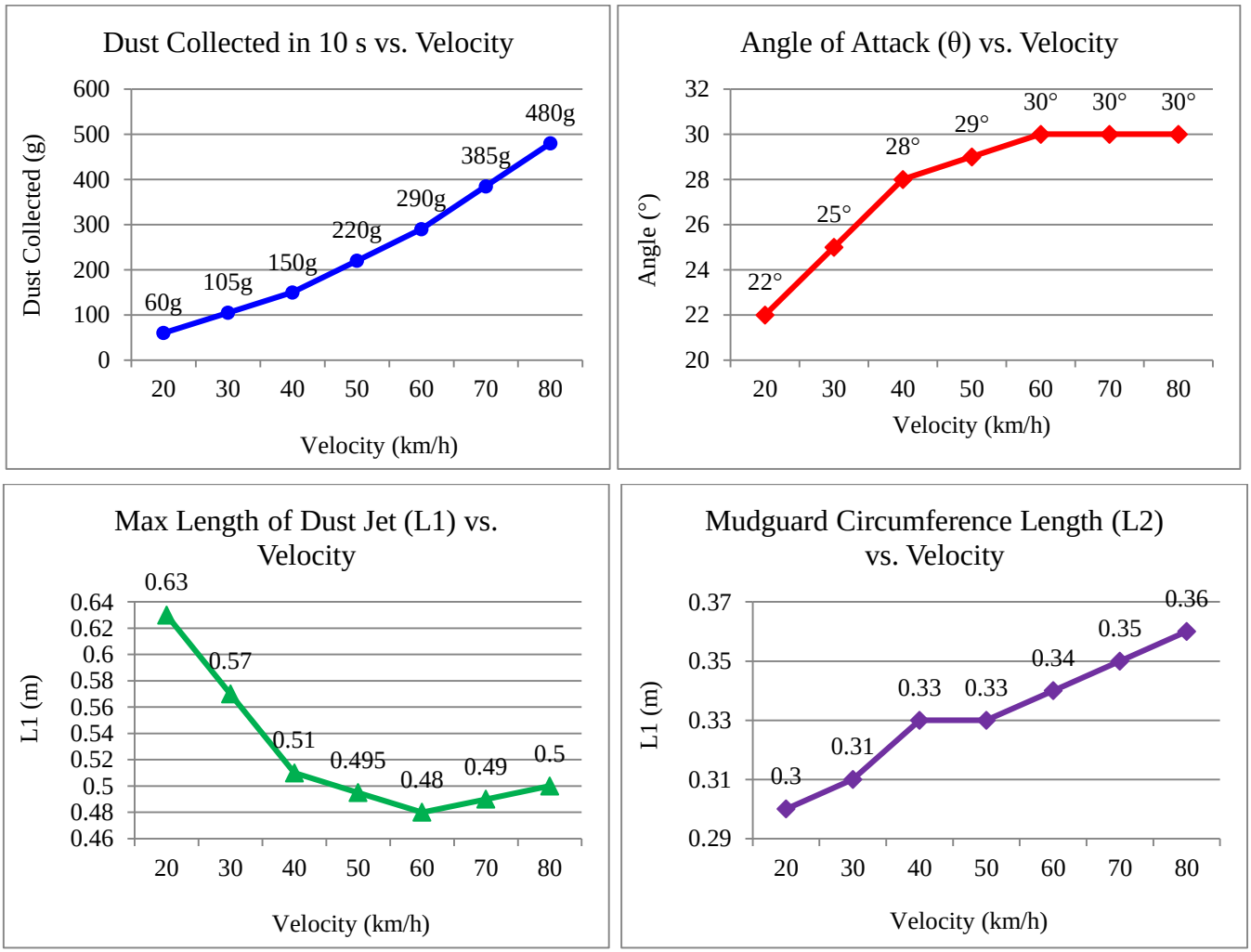



**Fig. 24 Correlation between vehicle velocity, mass of collected dust in 10 sec sampling and the resulting dust jet angle of attack**

The dust collection rate increases substantially from 60 g at 20 km/h to 480 g at 80 km/h (Figure 24), showing a strong positive relationship with vehicle speed. The angle of attack (θ) increases from 22° at 20 km/h and stabilizes at approximately 30° from 60 to 80 km/h. The maximum dust jet length ($L_1$) decreases from 0.63 m at 20 km/h to a minimum of 0.48 m at 60 km/h, followed by a slight increase to 0.50 m at 80 km/h. The mudguard circumference jet length ($L_2$) increases progressively from 0.30 m to 0.36 m with increasing vehicle speed. The filter diameter (D = 0.43 m), dust plume diameter ($D^d$ = 0.15 m), and mobile equipment length ($L^f$ = 0.30 m) remain constant throughout the tested speed range.

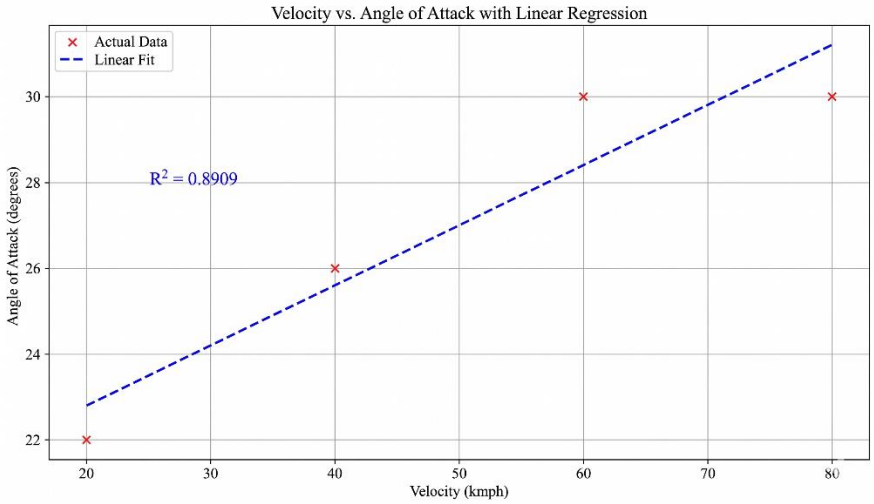



**Fig. 25 Angle of attack vs Velocity**

The variation in the angle of attack at different vehicle speeds, ranging from 20 to 80 km/h, is shown in Figure 25. The results indicate that the angle of dust movement generally increases with vehicle speed. At 20 km/h, the measured angle is 22°, suggesting that most of the dust remains close to the road surface with limited upward movement. When the speed increases to 40 km/h, the angle rises to 28°, which can be attributed to the stronger airflow generated by the moving vehicle. At 60 and 80 km/h, the angle reaches approximately 30° and remains nearly constant. This indicates that beyond a certain vehicle speed, further increases in velocity have only a limited effect on the dust trajectory.

The relationship between vehicle velocity (x) and the corresponding angle of attack is presented in Figure 25. A linear fit to the experimental results gives an $R^2$ value of 0.8909, indicating a strong relationship between vehicle speed and angle of attack within the investigated range. The linear equation obtained using the machine learning approach is presented in Equation. (3).

$$Y = -1.5x + 10.1x + 13.5 \quad (3)$$

The distance of the dust jet from the mudguard is calculated and given in Figure 26 at various speeds. It shows the variation of maximum dust length $L_1$ and $L_2$ (Y) for 20 KMPH speed of the vehicle (x), and the polynomial equations given are Equation. 4 & Equation. 5 with $R^2$ = 0.9942 and $R^2$ = 0.962, respectively. There is a variation of 3.17% mud guard circumference between $L_1$ and $L_2$.

$$Y = -0.035x2 + 0.21x + 0.81 \quad (4)$$

The experimental results show that vehicle speed strongly affects road-dust generation and dispersion behind the two-wheeler. As speed increased from 20 to 80 km/h, the collected dust rose from 60 to 480 g in 10 s, representing an eight-fold increase. The dust jet also expanded with increasing speed, while the angle of attack increased from 22° to about 30° at 60–80 km/h. The fitted relationships showed strong correlations, with $R^2$ values of 0.9751, 0.9734, 0.9942, and 0.9620. These results indicate that vehicle speed significantly influences both the quantity and spatial dispersion of resuspended road dust under the tested WBM-road conditions.

$$Y = 0.091x + 0.285 \quad (5)$$

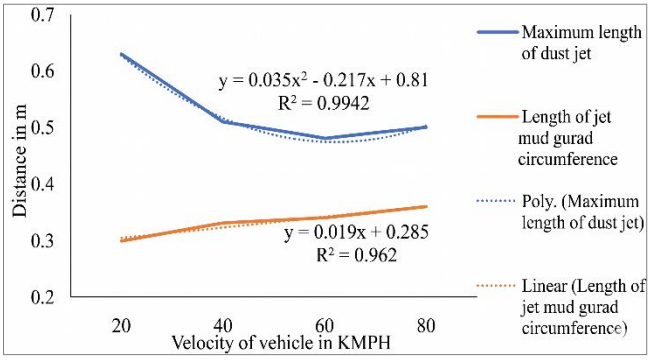



**Fig. 26 Length of jet mud guard for 20KMPH**

### *4.2. Machine Learning Models (Random Forest and XG Boost)*

Random Forest (RF) and XGBoost (XGB) regression models were used to analyse the experimental data and

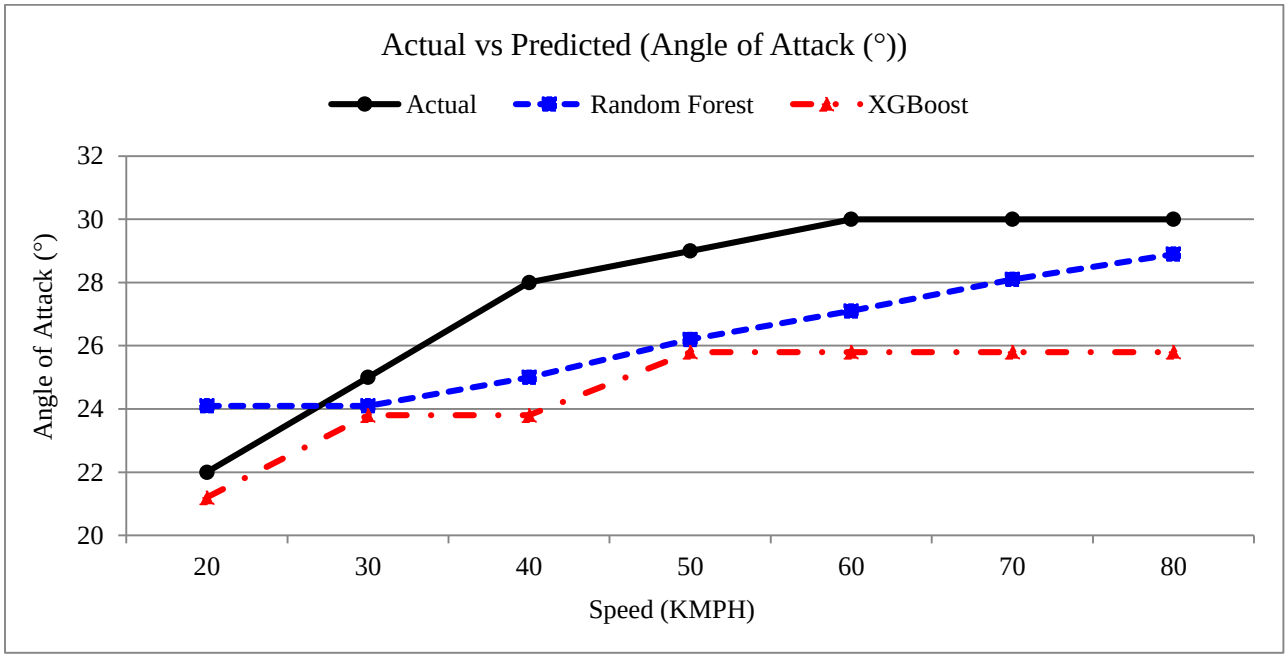
estimate the response values at 10 km/h intervals. The models were used to predict dust collected, angle of attack, and maximum jet length over the investigated speed range.

Both models produced consistent predictions with the experimental trend. The predicted angle of attack increased gradually with vehicle speed, while the maximum jet length also increased at higher speeds. The predicted dust collection showed a rapid increase with speed, which is consistent with the greater turbulence, airflow, and dust resuspension expected at higher vehicle velocities.

**Table 7. Machine learning models with different parameters**

| Speed (KMPH) | Angle of attack | | | Max Jet Length | | | Dust Collected | | |
|---|---|---|---|---|---|---|---|---|---|
| | Actual | RF | XGB | Actual | RF | XGB | Actual | RF | XGB |
| 20 | 22 | 24.1 | 21.2 | 0.63 | 0.431 | 0.420 | 60 | 133 | 55.576 |
| 30 | 25 | 24.1 | 23.8 | 0.57 | 0.431 | 0.453 | 110 | 133 | 143.499 |
| 40 | 28 | 25.0 | 23.8 | 0.51 | 0.446 | 0.453 | 150 | 160 | 143.499 |
| 50 | 29 | 26.2 | 25.8 | 0.49 | 0.462 | 0.482 | 210 | 206 | 265.509 |
| 60 | 30 | 27.1 | 25.8 | 0.48 | 0.471 | 0.482 | 290 | 248 | 265.509 |
| 70 | 30 | 28.1 | 25.8 | 0.49 | 0.481 | 0.500 | 395 | 314 | 383.225 |
| 80 | 30 | 28.9 | 25.8 | 0.50 | 0.489 | 0.500 | 480 | 390 | 383.225 |

The prediction models presented in Table 7 help extend the experimental dataset and provide additional information that can support further research and practical applications. The reliability of the models was evaluated using the correlation coefficient ($R^2$), which indicates the degree of agreement between the predicted and experimental values. A comparison of the actual experimental results with the predictions from the Random Forest (RF) and XGBoost (XGB) models was carried out to assess their ability to predict dust collection under different aerodynamic conditions. The experimental responses were mainly influenced by vehicle speed, angle of attack, and maximum jet length. The RF model, which combines multiple decision trees, can represent nonlinear relationships among these variables, whereas XGB uses a sequential boosting approach to reduce prediction errors. Both models followed the general experimental trends, although some differences were observed between the measured and predicted values. These deviations indicate that the prediction performance should be assessed using statistical measures such as $R^2$, RMSE, and MAE. Overall, the use of RF and XGB provides a useful approach for estimating dust collection behaviour, reducing the need for repeated experimental trials, and supporting the optimisation of aerodynamic design (Figure 27).



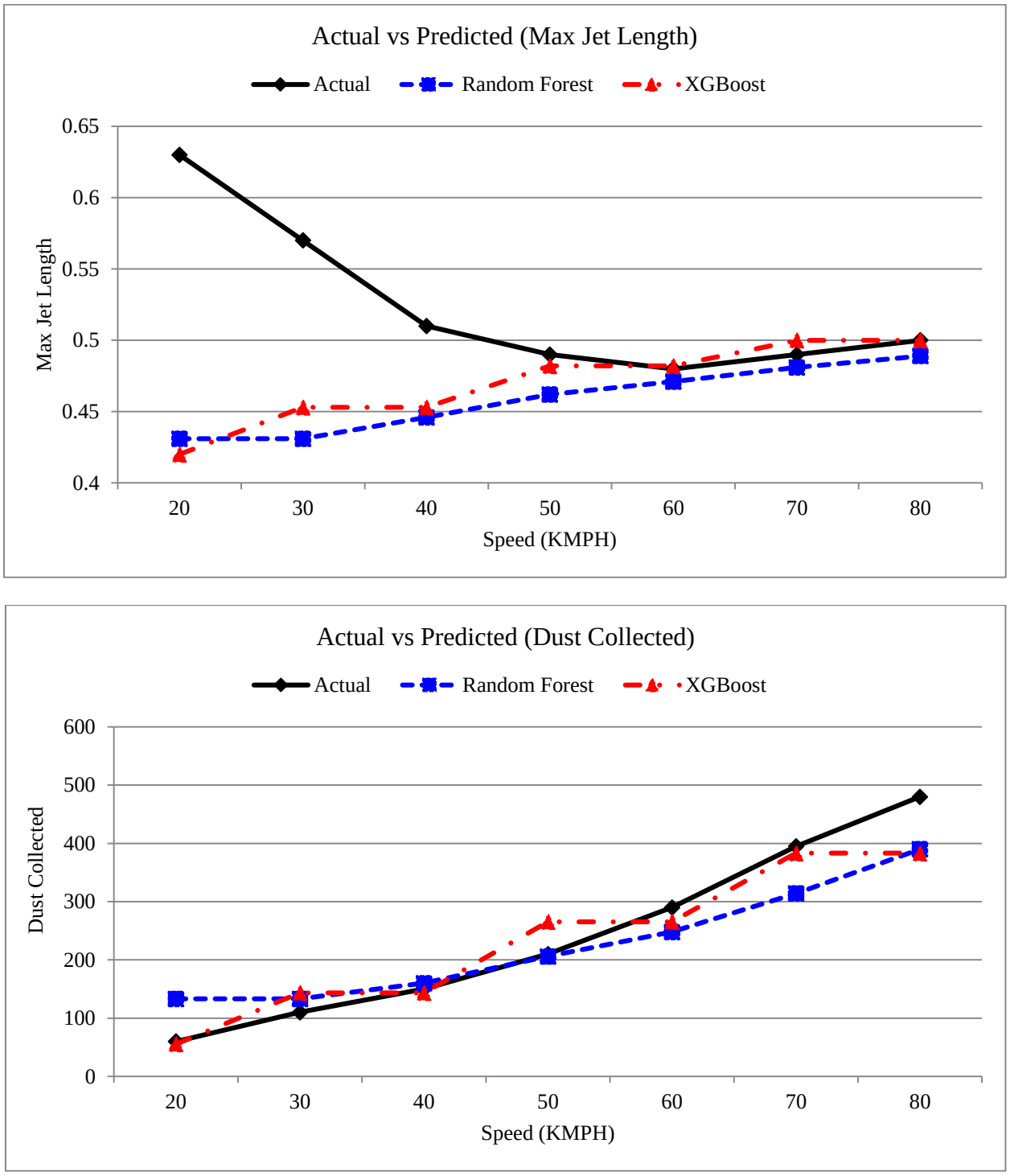



**Fig. 27 Model Functioning Pattern of each parameter (Angle of Attack, Dust Collected, and Max Jet Length) with Random Forest (RF) and XGBoost (XGB)**

For the angle of attack, the RF model showed better agreement with the experimental observations, with an RMSE of 2.2453, MAE of 2.1000, and $R^2$ of 0.3855. In contrast, the XGB model produced an RMSE of 3.4409, MAE of 3.1429, and a negative $R^2$ of −0.4432, indicating a lower ability to represent the observed variation in angle of attack. Based on these statistical indicators, the RF model provided a closer representation of the experimental variation in aerodynamic angle with vehicle speed.

For dust collection, both models showed limited predictive performance in terms of $R^2$. The RF model produced an RMSE of 0.0959, MAE of 0.0663, and $R^2$ of −2.5673, whereas XGB produced an RMSE of 0.0936, MAE of 0.0584, and $R^2$ of −2.3967. The detailed results are presented in Table 8. The negative $R^2$ values indicate that the models were unable to adequately explain the variation in the dust-collection data, which may be associated with the limited experimental dataset, measurement sensitivity, and nonlinear aerodynamic effects. Nevertheless, the relatively small RMSE and MAE values indicate that the predicted dust values remained reasonably close to the measured values in absolute terms. These results suggest that, while the models have limitations in explaining the overall variation, they can still provide useful estimates within the range of the experimental observations.

**Table 8. The comparison of different parameters with different models and their interpretation**

| Parameter | Model | RMSE | MAE | $R^2$ | Interpretation |
|---|---|---|---|---|---|
| Angle of attack (°) | RF | 2.2453 | 2.1000 | 0.3855 | Moderate accuracy; RF captures the actual trend fairly well. |
| | XGB | 3.4409 | 3.1429 | -0.4432 | Poor performance; unable to follow experimental variation. |
| Dust Collected (g ) | RF | 0.0959 | 0.0663 | -2.5673 | Low RMSE/MAE but negative $R^2$ indicates limited correlation. |
| | XGB | 0.0936 | 0.0584 | -2.3967 | Slightly better than RF in error magnitude, but weak fit. |
| Max Jet Length (mm) | RF | 55.1802 | 46.8571 | 0.8480 | Excellent prediction; strong correlation with experimental data. |
| | XGB | 58.9515 | 49.6764 | 0.8272 | Good correlation, but slightly less accurate than RF. |

For the maximum jet length, the Random Forest (RF) model showed the strongest overall performance, with an RMSE of 55.1802, an MAE of 46.8571, and an $R^2$ of 0.8480. The high $R^2$ value indicates a strong agreement between the predicted and experimental values. The XGBoost (XGB) model also followed the experimental trend; however, the RF model represented the increase in jet length with vehicle speed more consistently across the investigated speed range.

Overall, the RF model showed better predictive performance than XGB for the aerodynamic parameters considered, particularly for angle of attack and maximum jet length. For dust collection, both models produced relatively similar prediction results. The RF model also showed more consistent behaviour with the experimental observations, indicating its usefulness for analysing dust collection and aerodynamic characteristics of two-wheeler vehicles.

The prediction accuracy of the regression models for dust collection at different vehicle speeds is further illustrated in Figure 27. The figure compares the actual dust collected with the values predicted by the regression models at 10 km/h intervals. The corresponding $R^2$ values obtained from the linear regression equations (Equations. 6 and 7) indicate the degree of agreement between the experimental and predicted results and provide an additional assessment of model performance.

The actual dust collection regression line is given in Equation. 6

$$Y = 6.5x + 15, R2 = 0.98 \quad (6)$$

Likewise, the anticipated dust accumulation is given in Equation. 7

$$Y = 6.4x + 14, R2 = 0.97 \quad (7)$$

The little discrepancy between actual and predicted values suggests that the models—Random Forest and XGBoost, for example accurately capture the relationship between dust accumulation (Y) and speed (x). Figure 27 shows the agreement between the actual and ML-predicted dust characteristics.

Figure 29 presents a heatmap illustrating the relationship between vehicle speed and the investigated parameters. The angle of attack, jet length, and dust collected over 10 seconds increase with speed, with the highest dust collection observed at 80 km/h. This trend is consistent with studies reporting the influence of vehicle-induced turbulence on particulate dispersion [45, 46]. In contrast, dust diameter and dust collector length remain nearly constant, indicating limited sensitivity to vehicle speed. The heatmap also shows similar trends for jet length, mudguard circumference, and dust collection.

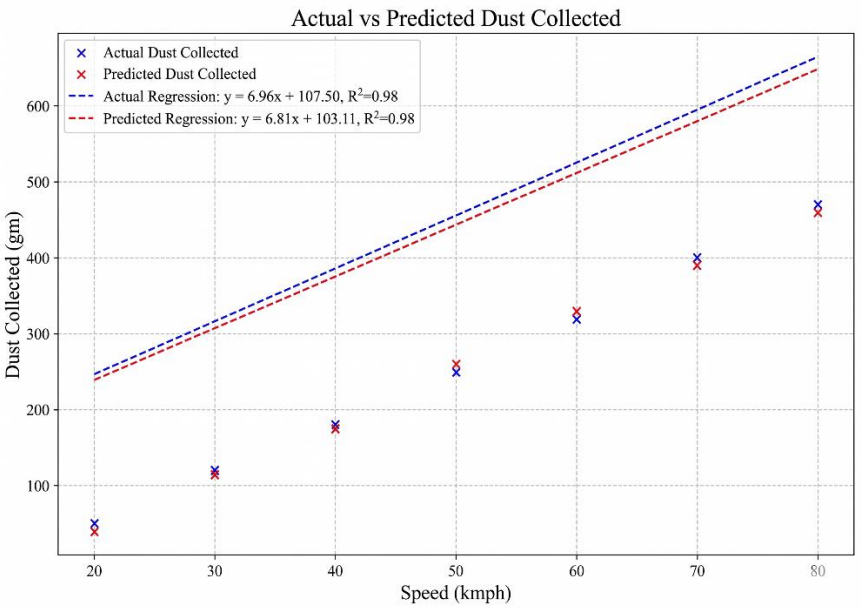



**Fig. 28 Actual vs predicted dust collected**

**Table 9. Relationship between collected dust and speed**

| Aspect | Expression / Formula | Interpretation / Remarks |
|---|---|---|
| Hourly Dust Collection | Hourly Dust $\propto V^n$ | Dust suspension increases with vehicle speed. The exponent $n$ depends on road type: Gravel (high $n$), Asphalt (moderate $n$), and Concrete (low $n$). |
| Dust Collected Over Time | $D(t) = f(V,R) \cdot t$ | The total dust collected over time depends on the speed (V) and type of road (R). Function $f(V,R)$represents the hourly dust collection rate. |
| Dust Collected Over Distance | $D(d) = [\frac{f(V,R)}{V}] \cdot d$ | Since dust per kilometer is derived by dividing the hourly dust collection rate by speed. |
| Simplified Time-Based Relation | $D(t) = k \cdot V^n \cdot t$ | Combines speed and time into a single expression. Constant $k$ includes road-dependent factors. |
| Simplified Distance-Based Relation | $D(d) = k \cdot V^{(n-1)} \cdot d$ | |

**Table 10. Numerical estimation of different parameters**

| Speed (km/h) | Velocity (m/s) | Distance (m) | Time (s) | Acceleration (m/s²) | Mass (kg) | Force (N) |
|---|---|---|---|---|---|---|
| 10 | 0.134852 | 0.58 | 4.300999806 | 0.031353725 | 1.38683E-12 | 4.34824E-14 |
| 20 | 0.234792 | 0.63 | 2.683230496 | 0.087503331 | 1.38683E-12 | 1.21353E-13 |
| 30 | 0.324755 | 0.57 | 1.755170373 | 0.185027507 | 1.38683E-12 | 2.56602E-13 |
| 40 | 0.408796 | 0.52 | 1.272028314 | 0.321373296 | 1.38683E-12 | 4.45691E-13 |
| 50 | 0.488691 | 0.495 | 1.012909451 | 0.482462932 | 1.38683E-12 | 6.69096E-13 |
| 60 | 0.568587 | 0.48 | 0.844198585 | 0.673522327 | 1.38683E-12 | 9.34063E-13 |
| 70 | 0.661520 | 0.49 | 0.740718473 | 0.893078693 | 1.38683E-12 | 1.23855E-12 |
| 80 | 0.681020 | 0.5 | 0.734192828 | 0.927576481 | 1.38683E-12 | 1.28639E-12 |

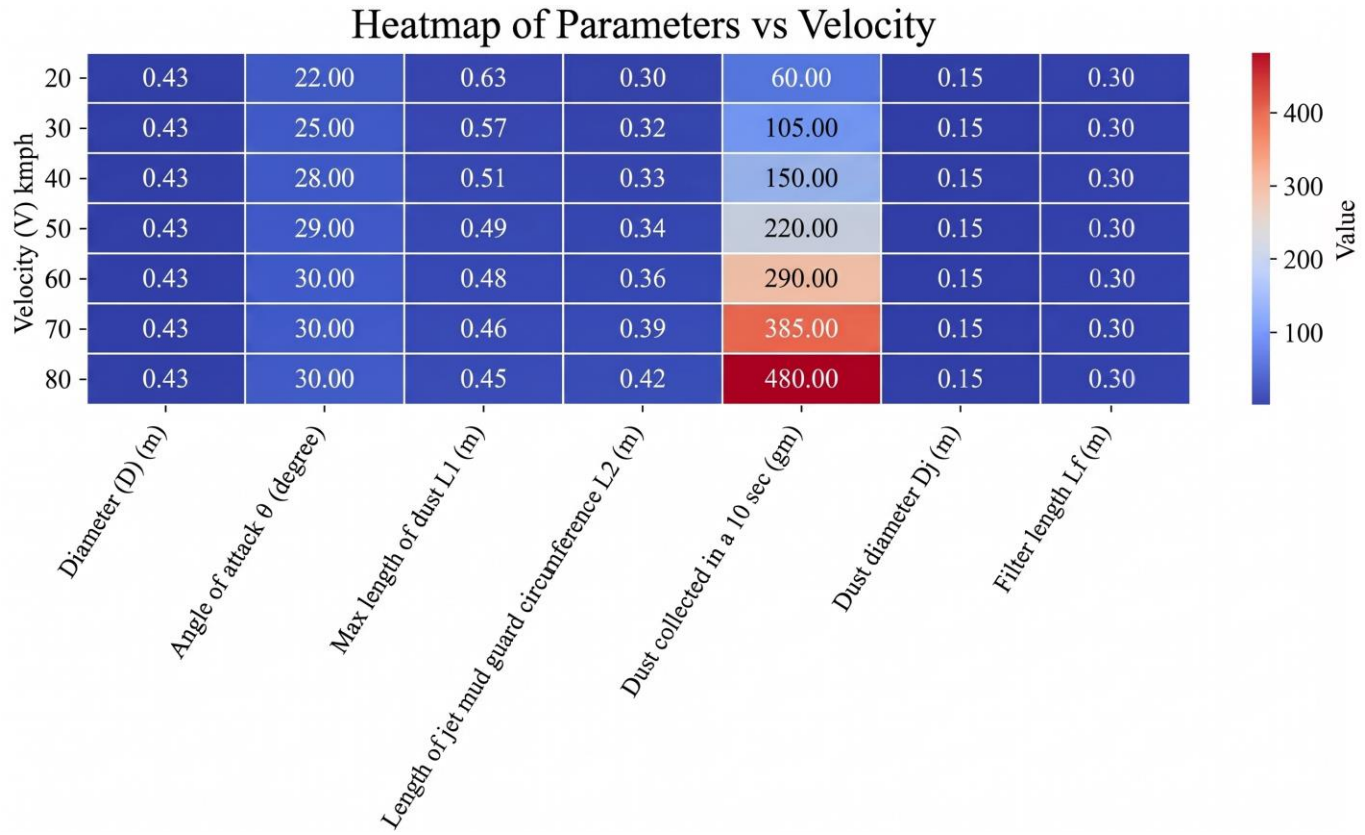



**Fig. 29 Heat map of different parameters with velocity**

### *4.3. Relation between Time, Distance, Dust Collected, and Vehicle Speed*

The dataset includes vehicle speed, dust collected, and associated parameters. By examining these, one can derive a mathematical relationship between vehicle speed (V), hourly dust collected (D), time (t), and distance travelled by vehicle (d). Understanding these relationships is crucial for comprehending the patterns of dust emissions on various road surfaces, including gravel, asphalt, and concrete.

#### *4.3.1. The Relationship between Collected Dust and Speed*

Vehicle speed determines how much dust is collected in a given amount of time. Dust suspension increases as vehicle speed rises. This is illustrated in Table 9.

#### *4.3.2. A Detailed Analysis of the Data on Mass, Force, Acceleration, Time, Distance, Vehicle Speed and Dust Particle Velocity*

The data in Table 10 shows how the speed of the vehicle affects the motion of dust particles. The relation between acceleration, dust particle velocity, vehicle speed, and the force exerted on a microscopic particle of the dust is the primary motivation of the study.

By calculating this relationship, it becomes simpler to identify how dust particles behave in various road and traffic conditions.

The speed of the vehicle is used to measure the motion of dust particles. The range of speeds is 10 to 80 km/h. The speed at which the particle moves, expressed in metres per second. As the speed of the vehicle increases, it increases steadily. Dust particles fluctuate slightly due to variations in turbulence and airflow. How long does it take the particle to cover the specified distance? As speed rises, indicating faster motion of dust particles.

The rate at which velocity changes over time. Acceleration values increase as vehicle speeds increase. It is common for airborne particles of PM2.5 and PM10 size, the assumed mass of the dust particle is $1.38683\times10^{-12}$ kg. Newton's Second Law ($F = m \times a$) is used to compute the force operating on the dust particle. As the acceleration increases, it climbs. The analysis indicates that both acceleration and the force acting on the dust particle increase with the vehicle's speed. This occurs because the greater airflow generated by the faster-moving vehicles produces more drag and tangential force on the dust particles. The values of forces fall within the range of pico-newtons, which is suitable for small particles, such as those with a diameter of PM2.5 and PM10. Greater acceleration yields higher resultant forces, even though the mass of the dust particle remains constant. Designing dust collector and assessing dust motion near roads is made simpler with the information given in Table 10.

## 5. Performance Investigation of the Dust Collector

To evaluate the effectiveness of the dust collector, a test was conducted at various vehicle speeds and road types. The velocity of dust particles is estimated using Equation. (8). The effectiveness or efficiency of the dust collection is estimated by using Equation. (9).

$$Velocity\ of\ Dust = (0.1 * Velocity\ speed^{0.8}) * (Silt\ Content)^{0.5} * (1 - Moisture\ Content)^{0.6} * Road\ Roughness\ Factor\ [58 - 63] \quad (8)$$

$$Efficiency = \frac{M_1 - M_2}{M_1} \quad (9)$$

Where $M_1$: Mass Inflow
$M_2 = M_1$ – Dust Collected

### *5.1. Dust Collected Data of Gravel Road*

Table 11 presents a detailed calculation of the dust collection efficiency of the dust collector and its associated parameters for a gravel road at various vehicle speeds, ranging from 10 km/h to 50 km/h. The percentage efficiency of the dust collector increases gradually with speed, starting from 55.57% at 10 km/h and reaching 67.29% at 50 km/h. The dust mass inflow (M1) values represent the total amount of dust entering the system. Similarly, the dust mass outflow (M2) shows dust that has not been collected. The dust collected (kg) by the equipment also increases from 2.92 kg to 5.67 kg as vehicle speed increases, indicating improved collection performance at higher velocities. The dust particle velocity in the air suggests a proportional increase with the vehicle's speed, rising from 0.1348 m/s at 10 km/h to 0.4887 m/s at 50 km/h. The factor of road roughness remains constant at 0.6 for all conducted tests, while both silt content (0.13%) and moisture content (0.02%) remain consistent throughout the experiments. The experimentally measured dust collected per hour (kg/hr) indicates a stable increase from 0.0073kg/hr at 10 km/hr to 0.0285 kg/hr at 50 km/hr. Likewise, the model-forecast values follow the same trend, ranging from 0.007571 to 0.030411 kg/hr. The percentage error between experimental values and mathematical model-predicted values varies marginally, ranging from 3.58% to 6.36%, indicating a good agreement between the experimental values and the mathematical model-predicted values. So finally, for the Gravel Road, the regression equation is derived and is given by Equation. (10).

$$D_c = 0.001861 + 0.000571V_s, \quad (R^2 = 99.31\%) \quad (10)$$

Whereas Dc stands for dust collected (kg/hr) and Vs stands for vehicle speed (km/hr). This correlation indicates that the rate of dust collection increases linearly with the vehicle's speed, confirming that higher speeds generate more fugitive dust due to increased turbulence and road surface contact.

**Table 11. Dust collected data of Gravel Road**

| **% Efficiency** | **55.57%** | **62.27%** | **64.15%** | **67.20%** | **67.29%** |
|---|---|---|---|---|---|
| Dust Mass Outflow (M2) | 2.33 | 1.92 | 2.52 | 3.48 | 2.77 |
| Dust Collected (kg) | 2.920 | 3.165 | 4.510 | 7.13567 | 5.695 |
| Dust Mass Inflow (M1) (kg) | 5.25 | 5.08 | 7.03 | 10.62 | 8.46 |
| Velocity of Dust (m/s) | 0.134852366 | 0.234791607 | 0.324754798 | 0.408795932 | 0.488691264 |
| Vehicle Speed (km/hr) | 10 | 20 | 30 | 40 | 50 |
| Silt Content (%) | 0.13 | 0.13 | 0.13 | 0.13 | 0.13 |
| Moisture Content (%) | 0.02 | 0.02 | 0.02 | 0.02 | 0.02 |
| Road Roughness Factor | 0.6 | 0.6 | 0.6 | 0.6 | 0.6 |
| Dust Collected per hr (kg/hr) EXP | 0.73 | 1.266 | 1.804 | 2.37 | 2.8475 |
| Dust Collected (kg/hr) Model | 0.7571 | 1.3281 | 1.8991 | 2.4701 | 3.0411 |
| Dc (kg/hr) = 0.001861 + 0.000571 Vs (km/hr) | | | | | |

**Table 12. Dust Collected on Asphalt Road**

| % Efficiency | 50% | 57.64% | 62.55% | 64.16% | 65.54% |
|---|---|---|---|---|---|
| Dust Mass Outflow (M2) | 2.37 | 1.96 | 3.83 | 3.46 | 3.32 |
| Dust Collected (kg) | 2.41 | 2.665 | 6.4 | 6.197 | 6.307 |
| Dust Mass Inflow (M1) (kg) | 4.78 | 4.62 | 10.23 | 9.66 | 9.62 |
| Velocity of Dust (m/s) | 0.1227 | 0.213565 | 0.29539496 | 0.371838254 | 0.444510555 |
| Vehicle Speed (km/hr) | 10 | 20 | 30 | 40 | 50 |
| Silt Content (%) | 0.08 | 0.08 | 0.08 | 0.08 | 0.08 |
| Moisture Content (%) | 0.03 | 0.03 | 0.03 | 0.03 | 0.03 |
| Road Roughness Factor | 0.7 | 0.7 | 0.7 | 0.7 | 0.7 |
| Dust Collected per hr (kg/hr) EXP | 0.535 | 1.066 | 1.6 | 2.06 | 2.522 |
| Dust Collected per hr (kg/hr) Model | 0.5664 | 1.095 | 1.624 | 2.1536 | 2.6824 |
| Dc (kg/hr) = 0.000374 + 0.000529 Vs (km/hr) | | | | | |

### *5.2. Dust Collected on Asphalt Road*

Table 12 summarises the dust collection performance at vehicle speeds of 10–60 km/h on an asphalt road. Collection efficiency increased from 50% at 10 km/h to 65.65% at 60 km/h, while dust collected increased from 2.41 to 7.31 kg. Dust particle velocity also increased from 0.1227 to 0.5143 m/s. The silt and moisture contents were 0.08% and 0.03%, respectively, with a road roughness factor of 0.7.

The experimentally determined dust collection rate increased from 0.00536 to 0.02924 kg/h, while the mathematical predictions ranged from 0.005664 to 0.032114 kg/h. The percentage error between the experimental and predicted values varied from 1.47% to 8.96%, indicating close agreement. The relationship between vehicle speed and dust collection rate is represented by the regression equation given in Equation. (11).

$$D_c = 0.000374 + 0.000529V_s, \quad (R^2 = 98.80\%) \qquad (11)$$

This linear relationship indicates that dust collection increases proportionally with vehicle speed, confirming that higher vehicle speeds result in greater dust production and capture due to increased road surface disturbance and air turbulence.

### *5.3. Dust Collected on Concrete Road*

Table 13 summarises the dust collection performance on a concrete road at vehicle speeds of 10–50 km/h. Collection efficiency increased from 23.01% at 10 km/h to 33.26% at 50 km/h, while the dust collected increased from 2.2 to 3.2 kg. Dust particle velocity also increased from 0.1227 to 0.4445 m/s, reflecting greater air turbulence at higher speeds.

The experimental dust collection rate increased from 0.001913 to 0.0128 kg/h, while the mathematical predictions ranged from 0.001824 to 0.01366 kg/h. The percentage error varied between 2.96% and 6.4%, indicating close agreement between experimental and predicted values. The regression relationship for the concrete road is presented in Equation. (12).

$$D_c = -0.001136 + 0.000296V_s, \quad (R^2 = 98.30\%) \qquad (12)$$

This linear equation suggests that dust collection increases with the speed of the vehicle, while the overall rate remains lower compared to rougher surfaces, such as gravel roads or asphalt roads. This shows the smoother texture of concrete roads, which produces less loose dust for entrainment into the air.

**Table 13. Dust Collected on Concrete Road**

| **% Efficiency** | **23.01%** | **24.03%** | **26.30%** | **29.28%** | **33.26%** |
|---|---|---|---|---|---|
| Dust Mass Outflow (M2) | 7.36 | 12.64 | 10.37 | 7.97 | 6.42 |
| Dust Collected (kg) | 2.2 | 4.0 | 3.7 | 3.3 | 3.2 |
| Dust Mass Inflow (M1) (kg) | 9.56 | 16.64 | 14.07 | 11.27 | 9.62 |
| Velocity of Dust (m/s) | 0.122660879 | 0.213564995 | 0.295394958 | 0.37183825 | 0.444510555 |
| Vehicle Speed (km/hr) | 10 | 20 | 30 | 40 | 50 |
| Silt Content (%) | 0.08 | 0.08 | 0.08 | 0.08 | 0.08 |
| Moisture Content (%) | 0.03 | 0.03 | 0.03 | 0.03 | 0.03 |
| Road Roughness Factor | 0.7 | 0.7 | 0.7 | 0.7 | 0.7 |
| Dust Collected per hr (kg/hr) EXP | 0.1913 | 0.44 | 0.74 | 1.1 | 1.28 |
| Dust Collected per hr (kg/hr) Model | 0.1824 | 0.4784 | 0.7744 | 1.0704 | 1.366 |
| Dc (kg/hr) = -0.001136 + 0.000296 Vs (km/hr) | | | | | |

### *5.4. Principal Discovery of the Research Work*

The Figure 30 shows that the gravel Road (Water Bound Macadam Road) display the highest dust collection efficiency. It is about 3% more than the efficiency of an asphalt road and 35% more than a concrete road. Asphalt road shows moderate Performance of dust collection. It is about 3% less than a gravel road and 32% more than a concrete road. The performance of dust collector on a concrete road is about 30%, which is less than that of gravel and asphalt road. Dust collector efficiency for concrete road is less because the dust generation during the motion of vehicles on the concrete road is less. But the dust generated from concrete roads is chemical in nature and cause significant health risk to humans.

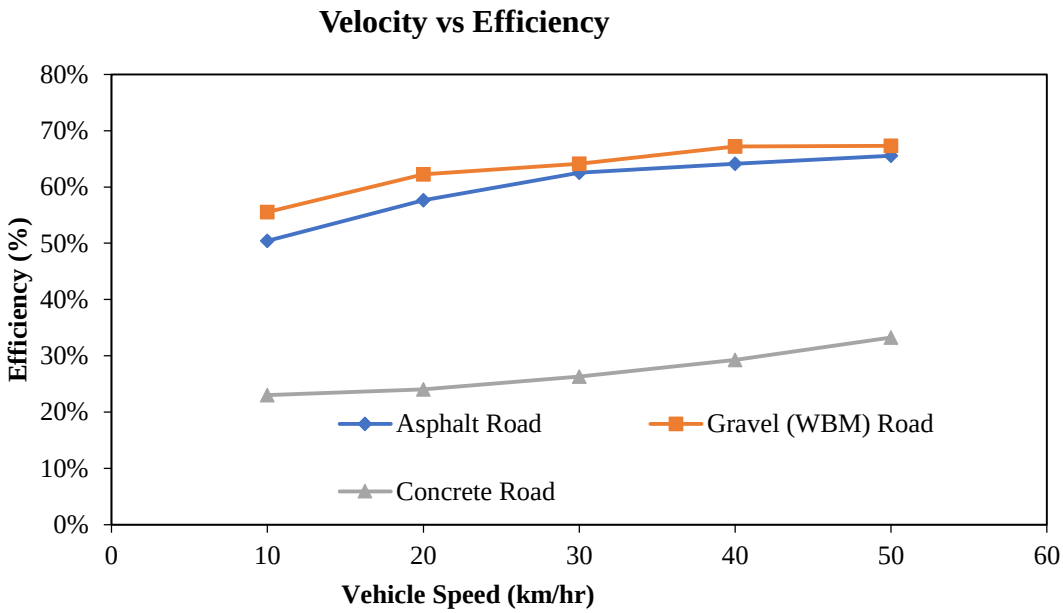



**Fig. 30 Velocity vs Efficiency**

### *5.5. Practical Applicability of the Developed Dust Collector*

In the regions of environmental observation and dust pollution control, the two-wheeler-installed dust-collecting sampler is highly relevant. Due to its small size and mobility, it can be used in roadside and real traffic situations where predictable, unmoving samplers or vacuum trucks are inconvenient. The equipment is helpful for research related to vehicle emissions, urban and rural air quality assessment, and dust load measurement on different road types, as it can be applied to both on-site particulate matter studies and actual road dust collection. The sampler is easily attached to any other two-wheeler without compromising vehicle functionality or balance. Another benefit is its low power consumption and lightweight construction. The dust collector is a user-friendly, easy to install on the vehicle, easy to maintain and cost-effective substitute for expensive, currently available commercial equipments in the markets.

### *5.6. Limitations of the Present Study*

Although it features an innovative design and practical suitability, the established prototype has some limitations.

a) The equipment collects dust in a dust collector without directly calculating the concentration or chemical composition.
b) Road conditions, wind direction, and vibration of a two-wheeler can also affect performance by disturbing dust collection and airflow.
c) Particle size distribution analysis was performed by sedimentation analysis according to ASTM D 7828-Standard test method for particle size distribution of fine-grained soil using hydrometer equipment, particularly for $PM_{2.5}$ and $PM_{10}$, as it is relevant to the objectives of the present study. However, SEM-EDS analysis was not included in the present experimental work, and elemental characterization is therefore proposed for future investigations.

### *5.7. Environmental Considerations and Dust Disposal*

To safeguard public health, address environmental concerns, and ensure proper dust disposal, focus on safely capturing particles, reducing air pollution, and handling the collected dust effectively. The following ways are used to handle dust disposal after dust collection:

a) The filter compartment, which is easily removable and clean, in which dust particles are trapped.
b) The filter catches PM2.5 and PM10 in the vicinity of the nearby vehicle.
c) The dust must be disposed of securely in municipal solid waste bins or garbage bins.
d) The equipment reduces secondary resuspension of the dust in the atmosphere because it exclusively collects and stores the dust.

## 6. Conclusion and Future Scope of Work

- A compact dust collector was designed and tested for the collection of road dust generated behind a two-wheeler. The prototype has a reported length of 0.3 m, a diameter of 0.15 m, an approximate weight of 2 kg, and an estimated fabrication cost of ₹7,500.
- The dust collection efficiency depends on the road surface. The reported efficiencies were 67.29% for gravel (water-bound macadam) roads, 65.65% for asphalt roads, and 33.26% for concrete roads. Under the tested conditions, the highest efficiency was recorded on gravel roads, whereas the lowest was observed on concrete roads.

- The amount of dust collected over a 10-second period increased from 60 g at 20 Km/h to 480 g at 80 km/h during testing on water-bound macadam roads. This shows that, under the experimental conditions, the measured dust accumulation increases with vehicle speed.
- The dust angle of attack increased from 22° at 20 km/h to approximately 30° at higher speeds. The maximum dust-jet length was 0.63 m at 20 km/h, decreased to 0.48 m at 60 km/h, and increased slightly to 0.50 m at 80 km/h.
- The empirical regression equations developed for gravel, asphalt, and concrete roads achieved reported $R^2$ values of 99.31%, 98.80%, and 98.30%, respectively. These results indicate a good fit to the data used to develop the equations. Further validation is required to assess their performance under other operating conditions.
- Among the machine-learning models, Random Forest (RF) performed better than XGBoost (XGB) in predicting the maximum dust-jet length. RF achieved an $R^2$ of 0.8480, while XGB achieved an $R^2$ of 0.8272. RF also recorded lower RMSE and MAE values for this parameter.
- For predicting the dust angle of attack, RF performed better than XGB based on the reported evaluation metrics. However, the $R^2$ value of 0.3855 for RF indicates that its predictive performance was limited.
- Both RF and XGB produced negative $R^2$ values for dust collection. This indicates that their predictions were inadequate compared with using the mean of the observed test values as a baseline. Therefore, further model development and validation are needed before these models can be considered suitable for predicting dust collection.
- The experimental findings demonstrate that the developed collector can be tested under different road surface and vehicle speed conditions. However, the study did not directly measure reductions in ambient $PM_{2.5}$ or $PM_{10}$ concentrations or evaluate human health benefits. Such outcomes cannot be confirmed from the present results.
- Further investigations should include repeated experiments, additional road surfaces, different vehicles, and independent validation datasets. These studies would help establish the consistency of dust collection efficiency and improve the predictive performance of the machine-learning models.

The designed collector provides a small, light, and reasonably priced option for testing dust collecting under various road and vehicle speed conditions as compared to previously reported road-dust sample methodologies. Although its effectiveness varies with road surface and operating speed, the trial findings show its capability for gathering road dust. To determine whether it performs better than current methods, more comparison testing under comparable circumstances is required.

### *6.1. Future Scope of Work*

The outcomes inspire the adoption of mobile dust collection systems in the automotive sector, promoting healthier and cleaner environments in both rural and urban areas. The limitation of stationary testing has been acknowledged, and dynamic road testing/CFD analysis has been identified as future work.

The mean, SD, CIs with the ANOVA testing for different ML models. The non-linear regression analysis or RSM method to be future analysed. To further enhance the dust collector's performance, future studies should investigate improved airflow dynamics and the use of advanced materials for filter design.

## Declaration

The authors assure that none of the work mentioned in this paper was motivated by any previously established contradictory financial interests or personal connections.

## Acknowledgment

Authors are grateful to the management of Bajaj Institute of Technology, Wardha for providing necessary support and infrastructure to conduct the present research work.

## Compliance with Ethical Standards

The authors declare no conflicts of interest regarding this manuscript. This paper does not involve human participants or animals.

I understand the provided information and have had the opportunity to ask questions. I know that my participation is voluntary and that I am free to withdraw at any time, without providing a reason and without incurring any costs. I voluntarily agree to take part in this study.

## Funding Statement

This study received no particular grants from public, commercial, or non-profit funding entities.

## Author Contributions

Dipak G. Mangrulkar is responsible for conceptualization, methodology, experimental investigation, data analysis, and writing (original draft preparation).

Prashant Y. Pawade provided experimental support, supervision, guidance, result interpretation, final manuscript review validation, and editing. All authors read and approved the final version of the manuscript.

Mangesh. P. Bhorkar provided experimental support, supervision, guidance, result interpretation, final manuscript review validation, and editing. All authors read and approved the final version of the manuscript.

## Ethics Approval

Thus, ethical approval was not necessary. The research followed institutional rules for academic research.

## Data Availability

The datasets generated and/or analysed during the current investigation are accessible from the corresponding author on reasonable request.

## Abbreviations

- PM Particulate Matter
- PVC Poly Vinyl Chloride
- HEPA High Efficiency Particulate Air Filter
- RPM Revolution per Minute
- WBM Water Bound Macadam

## References


[1] Thomas G. Sanders, and Jonathan Q. Addo, "Experimental Road Dust Measurement Device," *Journal of Transportation Engineering*, vol. 126, no. 6, 2000. [CrossRef] [Google Scholar] [Publisher Link]

[2] Joacim Lundberg et al., "Wet Dust Sampler—a Sampling Method for Road Dust Quantification and Analyses," *Water, Air, & Soil Pollution*, vol. 230, pp. 1-21, 2019. [CrossRef] [Google Scholar] [Publisher Link]

[3] Arpit Katiyar et al., "Fugitive Road Dust Particulate Matter Emission Inventory for India: A Field Campaign in 32 Indian Cities," *Science of the Total Environment*, vol. 912, 2024. [CrossRef] [Google Scholar] [Publisher Link]

[4] Shaofei Kong et al., "Risk Assessment of Heavy Metals in Road and Soil Dusts within PM2.5, PM10 and PM100 Fractions in Dongying City, Shandong Province, China," *Journal of Environmental Monitoring*, vol. 14, no. 3, pp. 791-803, 2012. [CrossRef] [Google Scholar] [Publisher Link]

[5] Theodoros Grigoratos, and Giorgio Martini, "*Non-Exhaust Traffic-Related Emissions. Brake and Tyre Wear PM*," EUR 26648 EN, European Commission, pp. 1-53, 2014. [CrossRef] [Google Scholar] [Publisher Link]

[6] Hyun-Min Hwang et al., "Review of Pollutants in Urban Road Dust: Part II. Organic Contaminants from Vehicles and Road Management," *International Journal of Urban Sciences*, vol. 23, no. 4, pp. 445-463, 2019. [CrossRef] [Google Scholar] [Publisher Link]

[7] Sharareh Dehghani, Farid Moore, and Razegheh Akhbarizadeh, "Microplastic Pollution in Deposited Urban Dust, Tehran Metropolis, Iran," *Environmental Science and Pollution Research*, vol. 24, no. 25, pp. 20360-20371, 2017. [CrossRef] [Google Scholar] [Publisher Link]

[8] Ida Järlskog et al., "Occurrence of Tire and Bitumen Wear Microplastics on Urban Streets and in Sweepsand and Washwater," *Science of the Total Environment*, vol. 729, pp. 1-13, 2020. [CrossRef] [Google Scholar] [Publisher Link]

[9] Joana Correia Prata, "Airborne Microplastics: Consequences to Human Health?," *Environmental Pollution*, vol. 234, pp. 115-126, 2018. [CrossRef] [Google Scholar] [Publisher Link]

[10] Enfeng Liu et al., "Pollution and Health Risk of Potentially Toxic Metals in Urban Road Dust in Nanjing, a Mega-City of China," *Science of the Total Environment*, vol. 476-477, pp. 522-531, 2014. [CrossRef] [Google Scholar] [Publisher Link]

[11] Theodoros Grigoratos, and Giorgio Martini, "Brake Wear Particle Emissions: A Review," *Environmental Science and Pollution Research*, vol. 22, no. 4, pp. 2491-2504, 2015. [CrossRef] [Google Scholar] [Publisher Link]

[12] Jana Kukutschová, and Peter Filip, *Chapter 6 - Review of Brake Wear Emissions: A Review of Brake Emission Measurement Studies: Identification of Gaps and Future Needs*, Non-Exhaust Emissions: An Urban Air Quality Problem for Public Health; Impact and Mitigation Measures, Academic Press, pp. 123-146, 2018. [CrossRef] [Google Scholar] [Publisher Link]

[13] Marisa L. Kreider et al., "Physical and Chemical Characterization of Tire-Related Particles: Comparison of Particles Generated using Different Methodologies," *Science of the Total Environment*, vol. 408, no. 3, pp. 652-659, 2010. [CrossRef] [Google Scholar] [Publisher Link]

[14] Julie M. Panko et al., "Measurement of Airborne Concentrations of Tyre and Road Wear Particles in Urban and Rural Areas of France, Japan, and the United States," *Atmospheric Environment*, vol. 72, pp. 192-199, 2013. [CrossRef] [Google Scholar] [Publisher Link]

[15] Pieter Jan Kole et al., "Wear and Tear of Tyres: A Stealthy Source of Microplastics in the Environment," *International Journal of Environmental Research and Public Health*, vol. 14, no. 10. pp. 1-31, 2017. [CrossRef] [Google Scholar] [Publisher Link]

[16] Kouji Adachi, and Yoshiaki Tainosho, "Characterization of Heavy Metal Particles Embedded in Tire Dust," *Environment International*, vol. 30, no. 8, pp. 1009-1017, 2004. [CrossRef] [Google Scholar] [Publisher Link]

[17] Stephan Wagner et al., "Tire Wear Particles in the Aquatic ENVIRONMENT - A Review on Generation, Analysis, Occurrence, Fate and Effects," *Water Research*, vol. 139, pp. 83-100, 2018. [CrossRef] [Google Scholar] [Publisher Link]

[18] M. Legret et al., "Leaching of Heavy Metals and Polycyclic Aromatic Hydrocarbons from Reclaimed Asphalt Pavement," *Water Research*, vol. 39, no. 15, pp. 3675-3685, 2005. [CrossRef] [Google Scholar] [Publisher Link]

[19] Peeyush Khare et al., "Asphalt-Related Emissions are a Major Missing Nontraditional Source of Secondary Organic Aerosol Precursors," *Science Advances*, vol. 6, no. 36, pp. 1-14, 2020. [CrossRef] [Google Scholar] [Publisher Link]

[20] Åsa Lindgren, "Asphalt Wear and Pollution Transport," *Science of the Total Environment*, vol. 189-190, pp. 281-286, 1996. [CrossRef] [Google Scholar] [Publisher Link]
[21] Patrik Fauser et al., "Quantification of Bitumen Particles in Aerosol and Soil Samples Using HP-GPC," *Petroleum Science and Technology*, vol. 18, no. 9-10, pp. 991-1007, 2000. [CrossRef] [Google Scholar] [Publisher Link]
[22] Patrik Fauser et al., "Tire-Tread and Bitumen Particle Concentrations in Aerosol and Soil Samples," *Petroleum Science and Technology*, vol. 20, no. 1-2, pp. 127-141, 2002. [CrossRef] [Google Scholar] [Publisher Link]
[23] Alistair Thorpe, and Roy M. Harrison, "Sources and Properties of Non-Exhaust Particulate Matter from Road Traffic: A Review," *Science of the Total Environment*, vol. 400, no. 1-3, pp. 270-282, 2008. [CrossRef] [Google Scholar] [Publisher Link]
[24] M.C Gromaire et al., "The Quality of Street Cleaning Waters: Comparison with Dry and Wet Weather Flows in a Parisian Combined Sewer System," *Urban Water*, vol. 2, no. 1, pp. 39-46, 2000. [CrossRef] [Google Scholar] [Publisher Link]
[25] Carla Candeias et al., "Geochemical, Mineralogical and Morphological Characterisation of Road Dust and Associated Health Risks," *International Journal of Environmental Research and Public Health*, vol. 17, no. 5. pp. 1-18, 2020. [CrossRef] [Google Scholar] [Publisher Link]
[26] C. A. Alves et al., "Chemical Profiling of PM10 from Urban Road Dust," *Science of the Total Environment*, vol. 634, pp. 41-51, 2018. [CrossRef] [Google Scholar] [Publisher Link]
[27] C. Perrino et al., "Particulate Matter Concentration and Chemical Composition in the Metro System of Rome, Italy," *Environmental Science and Pollution Research*, vol. 22, no. 12, pp. 9204-9214, 2015. [CrossRef] [Google Scholar] [Publisher Link]
[28] Inyong Park, Hongsuk Kim, and Seokhwan Lee, "Characteristics of Tire Wear Particles Generated in a Laboratory Simulation of Tire/Road Contact Conditions," *Journal of Aerosol Science*, vol. 124, pp. 30-40, 2018. [CrossRef] [Google Scholar] [Publisher Link]
[29] S. Potgieter-Vermaak et al., "Component-Specific Toxic Concerns of the Inhalable Fraction of Urban Road Dust," *Environmental Geochemistry and Health*, vol. 34, no. 6, pp. 689-696, 2012. [CrossRef] [Google Scholar] [Publisher Link]
[30] John F. Rosen, "Adverse Health Effects of Lead at Low Exposure Levels: Trends in the Management of Childhood Lead Poisoning," *Toxicology*, vol. 97, no. 1-3, pp. 11-17, 1995. [CrossRef] [Google Scholar] [Publisher Link]
[31] Lynn Marshall et al., "Identifying and Managing Adverse Environmental Health Effects: 1. Taking an Exposure History," *Canadian Medical Association Journal*, vol. 166, no. 8, pp. 1049-1055, 2002. [Google Scholar] [Publisher Link]
[32] Meredith Franklin, Petros Koutrakis, and Joel Schwartz, "The Role of Particle Composition on the Association Between PM2.5 and Mortality," *Epidemiology*, vol. 19, no. 5, pp. 680-689, 2008. [Google Scholar] [Publisher Link]
[33] Janneane F. Gent et al., "Symptoms and Medication Use in Children with Asthma and Traffic-Related Sources of Fine Particle Pollution," *Environmental Health Perspectives*, vol. 117, no. 7, pp. 1168-1174, 2009. [CrossRef] [Google Scholar] [Publisher Link]
[34] Margaret E. Farago et al., "Platinum Concentrations in Urban Road Dust and Soil, and in Blood and Urine in the United Kingdom," *Analyst*, vol. 123, no. 3, pp. 451-454, 1998. [CrossRef] [Google Scholar] [Publisher Link]
[35] Sujuan Xu et al., "Geochemistry and Health Risk Assessment of Arsenic Exposure to Street Dust in the Zinc Smelting District, Northeast China," *Environmental Geochemistry and Health*, vol. 35, no. 1, pp. 89-99, 2013. [CrossRef] [Google Scholar] [Publisher Link]
[36] Seung-Yoon Noh et al., "Comparison of Resuspended Road Dust Concentration for Identifying Optimum Sampling Position on a Mobile Laboratory Vehicle," *Aerosol Science and Technology*, vol. 55, no. 11, pp. 1230-1238, 2021. [CrossRef] [Google Scholar] [Publisher Link]
[37] J. Srinivas et al., "Computational Fluid Analysis(CFD) of Dust Collector using ANSYS," *International Journal of Research and Analytical Reviews*, vol. 7, no. 2, pp. 19-25, 2020. [Publisher Link]
[38] Xue Dong, "Design of a Filtering Car Air Purifier," *IOP Conference Series: Earth and Environmental Science: Asia Conference on Geological Research and Environmental Technology: Asia Conference on Geological Research and Environmental Technology*, Kamakura City, Japan, vol. 632, pp. 1-8, 2021. [CrossRef] [Google Scholar] [Publisher Link]
[39] Jamshid Valiev Fayzullayevich et al., "Improvement of Dust Particle Suction Efficiency by Controlling the Airflow of a Regenerative Air Sweeper," *Applied Sciences*, vol. 12, no. 19, pp. 1-25, 2022. [CrossRef] [Google Scholar] [Publisher Link]
[40] Yuan Xi et al., "Internal Flow Field Uniformity Study of Dust Collector for A Street Vacuum Sweeper Based on CFD," *IOP Conference Series: Materials Science and Engineering: 4th International Conference on Mechanical, Materials and Manufacturing*, Atlanta, USA, vol. 272, pp. 1-6, 2017. [CrossRef] [Google Scholar] [Publisher Link]
[41] Joseph I. Goldstein et al., *Scanning Electron Microscopy and X-Ray Microanalysis*, 4th ed., Springer, pp. 1-550, 2018. [CrossRef] [Google Scholar] [Publisher Link]
[42] Prashant Kumar et al., "A Review of Factors Impacting Exposure to PM2.5, Ultrafine Particles and Black Carbon in Asian Transport Microenvironments," *Atmospheric Environment*, vol. 187, pp. 301-316, 2018. [CrossRef] [Google Scholar] [Publisher Link]
[43] P. Kumar Mehta, and Paulo J. M. Monteiro, *Concrete: Microstructure, Properties, and Materials*, 4th ed., McGraw-Hill Education, 2014. [Google Scholar] [Publisher Link]
[44] Jiuzhu Wang et al., "Influence of Vehicle and Pavement Characteristics on Dust Resuspension from Soil Pavement of Open-pit Mine," *Science of the Total Environment*, vol. 878, 2023. [CrossRef] [Google Scholar] [Publisher Link]

[45] Ying Chen et al., "Mitigation of PM2.5 and Ozone Pollution in Delhi: A Sensitivity Study during the Pre-Monsoon Period," *Atmospheric Chemistry and Physics*, vol. 20, no. 1, pp. 499-514, 2020. [CrossRef] [Google Scholar] [Publisher Link]

[46] John H. Seinfeld, and Spyros N. Pandis, *Atmospheric Chemistry and Physics: From Air Pollution to Climate Change*, 3rd ed., Wiley, pp. 1-1152, 2016. [Google Scholar] [Publisher Link]

[47] V.V. Nandagopan, and Arpan Patra, How can mechanical road sweeping deliver cleaner air for Delhi's Citizens?, Council on Energy, Environment and Water, 2026. [Online]. Available: https://www.ceew.in/blogs/how-can-mechanical-road-sweeping-deliver-cleaner-air-delhi%E2%80%99s-citizens?

[48] Asanka de Silva et al., "Beyond Conventional Monitoring: A Semantic Segmentation Approach to Quantifying Traffic-Induced Dust on Unsealed Roads," *Sensors*, vol. 24, no. 2, pp. 1-15, 2024. [CrossRef] [Google Scholar] [Publisher Link]

[49] Dimitrinka Ivanova et al., "Predicting the Amount of Toxic Metals and Metalloids in Silt Loading using Neural Networks," *Environmental Monitoring and Assessment*, vol. 197, no. 4, 2025. [CrossRef] [Google Scholar] [Publisher Link]

[50] Lilai Song et al., "An Hourly and Localized Optimization Method for Soil Fugitive Dust Emission Inventory based on Machine Learning," *Journal of Environmental Sciences*, vol. 158, pp. 1-12, 2025. [CrossRef] [Google Scholar] [Publisher Link]

[51] Mengyuan Chu, and Huizhong Shen, "*Link-Level Mapping of Fugitive Road-Dust Emissions in Urban China Using Explainable Machine Learning and Open Traffic Data*," EGU General Assembly, EGU26-6623, 2026. [CrossRef] [Google Scholar] [Publisher Link]

[52] Yilin Wang et al., "Bayesian-optimized CNN-LSTM Neural Network for Predicting Road Construction Dust Concentrations," *Developments in the Built Environment*, vol. 25, pp. 1-21, 2026. [CrossRef] [Google Scholar] [Publisher Link]

[53] *AP-42: Compilation of Air Pollutant Emission Factors*, 13.2.2: Paved Roads, US Environmental Protection Agency, pp. 1-12, 2011. [Google Scholar] [Publisher Link]

[54] *AP-42: Compilation of Air Pollutant Emission Factors*, 13.2.2: Unpaved Roads, US Environmental Protection Agency, pp. 1-20, 2006. [Publisher Link]

[55] H. Kuhns et al., "Testing Re-Entrained Aerosol Kinetic Emissions from Roads: A New Approach to Infer Silt Loading on Roadways," *Atmospheric Environment*, vol. 35, no. 16, pp. 2815-2825, 2001. [CrossRef] [Google Scholar] [Publisher Link]

[56] H. Kuhns et al., "Testing Re-entrained Aerosol Kinetic Emissions from Roads: A New Approach to Infer Silt Loading on Roadways," *Atmospheric Environment*, vol. 35, no. 16, pp. 2815-2825, 2001. [CrossRef] [Google Scholar] [Publisher Link]

[57] Liisa Pirjola et al., "Road Dust Emissions from Paved Roads Measured Using Different Mobile Systems," *Journal of the Air & Waste Management Association*, vol. 60, no. 12, pp. 1422-1433, 2010. [CrossRef] [Google Scholar] [Publisher Link]

[58] Air Emissions Factors and Quantification, U.S. Environmental Protection Agency (EPA), 2006. [Online]. Available: https://www.epa.gov/air-emissions-factors-and-quantification/ap-42-fifth-edition-volume-i-chapter-13-miscellaneous-0

[59] Road Dust Emissions from Unpaved Surfaces: Guide to Reporting, 2020. [Online]. Available: https://www.canada.ca/en/environment-climate-change/services/national-pollutant-release-inventory/report/sector-specific-tools-calculate-emissions/road-dust-unpaved-surfaces-guide.html

[60] Mohammad Ahmad Alsheyab et al., "Modeling Dust Generation on Low-Volume Roads Based on Vehicle Speed and Surface Fines Content," *Journal of the Transportation Research Board*, vol. 2679, no. 1, pp. 435-449, 2025. [CrossRef] [Google Scholar] [Publisher Link]

[61] Ho-Jun Yoo et al., "Quantitative Assessment of Road Dust Suspension based on Variations in Asphalt Pavement Surface Texture," *Atmosphere*, vol. 16, no. 5, pp. 1-29, 2023. [CrossRef] [Google Scholar] [Publisher Link]

[62] Mark Sweeney et al., "Comparison of PI-SWERL with Dust Emission Measurements from a Straight-line Field Wind Tunnel," *Journal of Geophysical Research: Earth Surface*, vol. 113, no. F1, 2008. [CrossRef] [Google Scholar] [Publisher Link]

[63] Federal Highway Administration (FHWA), Mitigation of Particulate Emissions by Road Surface Treatments, U.S. Department of Transportation, 2007. [Online]. Available: https://www.fhwa.dot.gov/environment/air_quality/conformity/research/mpe_benefits/mpe07.cfm

## Appendix

**Table 1. Shows a comparison of existing road dust control technologies with the mobile dust collection sampler**

| Technology | Working Principle | Effectiveness | Cost Level | Environmental Impact | Maintenance Requirement | Advantages | Limitations | Suitable Road Types / Applications |
|---|---|---|---|---|---|---|---|---|
| Mechanical Street Sweeping | Rotating brushes collect coarse particles and debris into a hopper. | Moderate for large particles, less for fine dust. | Medium | Low, but may cause dust resuspension. | Frequent cleaning of brushes and bins. | Removes visible dirt and litter effectively. | Ineffective for fine suspended dust; requires a larger workforce. | Urban paved roads. |
| Vacuum / Suction Sweeping | High-powered vacuum collects dust into sealed hoppers. | high, particularly for PM2.5 and PM10 fine dust. | High | Minimal to low resuspension . | Filter maintenance and skilled operators are necessary. | Very effective for fine dust removal. | Expensive and less flexible for narrow roads. | Urban roads, airports, expressways. |
| Water Spraying / Flushing | Sprays water to wet road surfaces for temporary dust control. | High initially, lasts only a few hours. | Low | May cause water runoff and wastage. | Required frequent refilling and operation. | A quick and straightforward way to control dust. | Shorter time; uses water. | Unpaved or construction roads. |
| Chemical Dust Suppressants ($CaCl_2$, $MgCl_2$) | Retains surface moisture and binds dust particles. | High for unpaved roads. | Moderate | Risk of soil and groundwater contamination. | Needs periodic reapplication. | Long-lasting dust control. | Corrosive; not eco-friendly. | Gravel and haul roads. |
| Polymer / Bitumen Emulsion Stabilisers | Forms a thin binding film over surface particles. | High and durable. | Moderate –High | Depends on the chemical used; some are eco-safe. | Moderate; reapply after months. | Long-term dust suppression. | Requires skilled application; darkens surface. | Gravel and rural roads. |
| Vegetative Barriers (Grass / Tree Belts) | Plants trap airborne dust and reduce wind speed. | Moderate; depends on plant density. | Low | Environmentally positive. | Moderate (watering, trimming). | Improves aesthetics and air quality. | Needs space and maintenance. | Rural and suburban roadside areas. |
| Speed / Traffic Management | Limits vehicle speed and congestion to reduce dust. | Moderate; depends on user compliance. | Extremely Low | Good; no chemicals were utilised. | Poor (enforcement and signage). | Low-cost and straightforward method. | Depends on driver behaviour. | Construction zones, gravel roads. |

| | | | | | | | | |
|---|---|---|---|---|---|---|---|---|
| Paving / Surface Treatment | Converts loose road surface into bound pavement. | Very high and permanent. | Very High | Good; permanent solution. | Minimal once completed. | Persistent removal of dust. | High cost of building. | All of the major roads. |
| On-Vehicle Dust Sprayers / Vacuum Units | Vehicle-mounted sprayers or suction units clean surface dust. | Moderate. | High | Varies with the technology used. | Moderate upkeep. | While movements, active dust control . | High equipment and cost of energy . | Haul and mining roads. |
| Real-Time Fixed Monitoring Systems | Sensors continuously monitor particulate matter at fixed sites. | For monitoring only. | High | Impartial. | Moderate. | Provide continuous data on dust. | Not mobile; covers a limited area. | Urban and industrial zones. |
| Mobile Dust Collection Sampler (Two-Wheeler Mounted)-Present Study | Dust is collected during transportation by a compact suction and filter device. | High for dust capture in a particular area. | Very Low | Eco-friendly; no chemicals. | Easy to clean and replace filters. | Portable, low-cost, and provides real-time data. | Designed for data collection, not suppression. | All road types — urban and rural. |